TEXAS cosmology conference

Carbon Monoxide Line Emission as a CMB Foreground:

Tomography of the Star Forming Universe

Rashid Sunyaev

In collaboration with **Mattia Righi** and **Carlos Hernandez-Monteagudo**

Max-Planck-Institut für Astrophysik (MPA)
Space Research Institute (IKI), Moscow

October 29, 2009

CO rotational levels

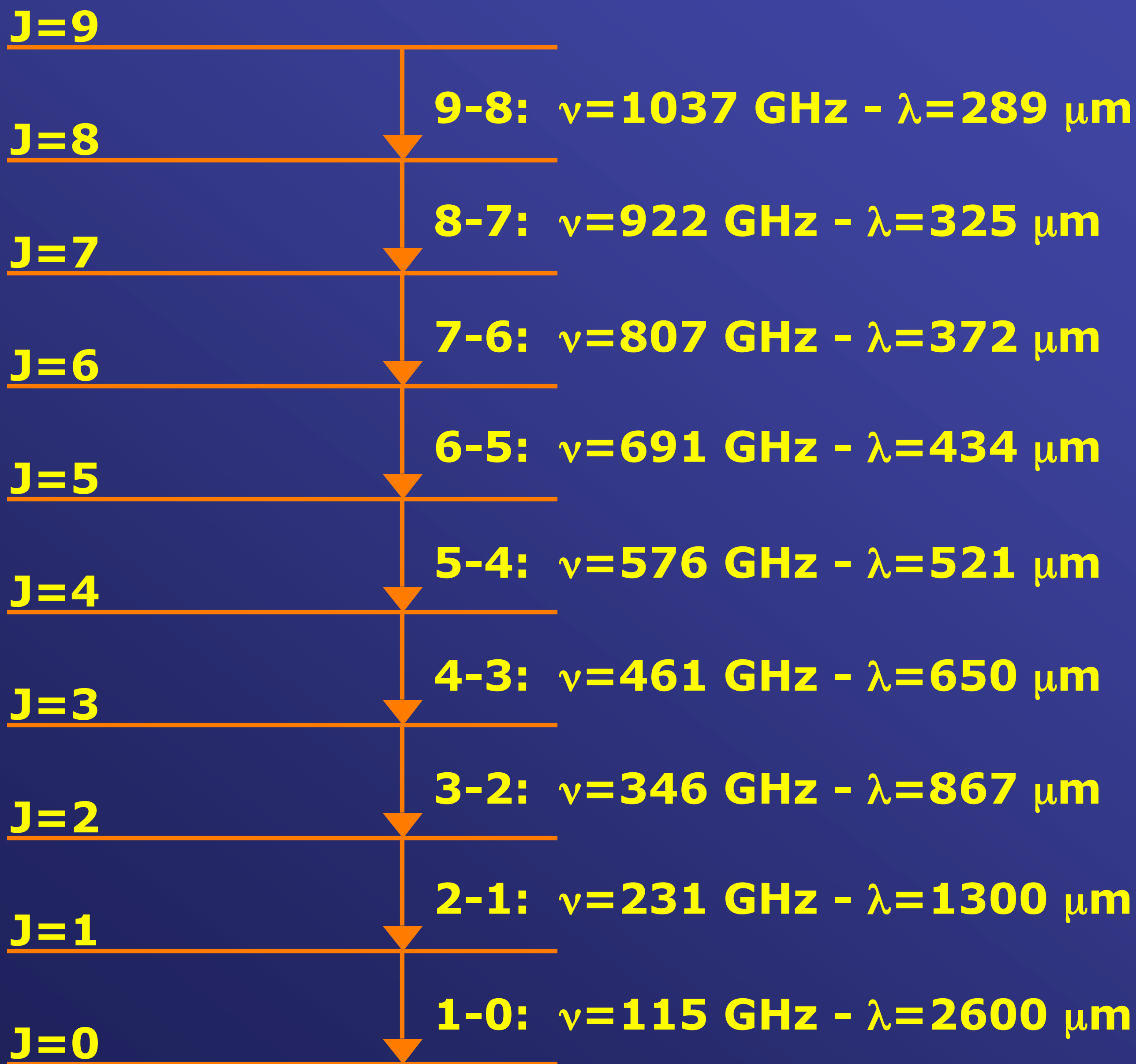

Population III stars produce very effectively C and O

Heger and Woosley, 2002

Are there traces of CO emission in early Universe on CMB maps?

- practically

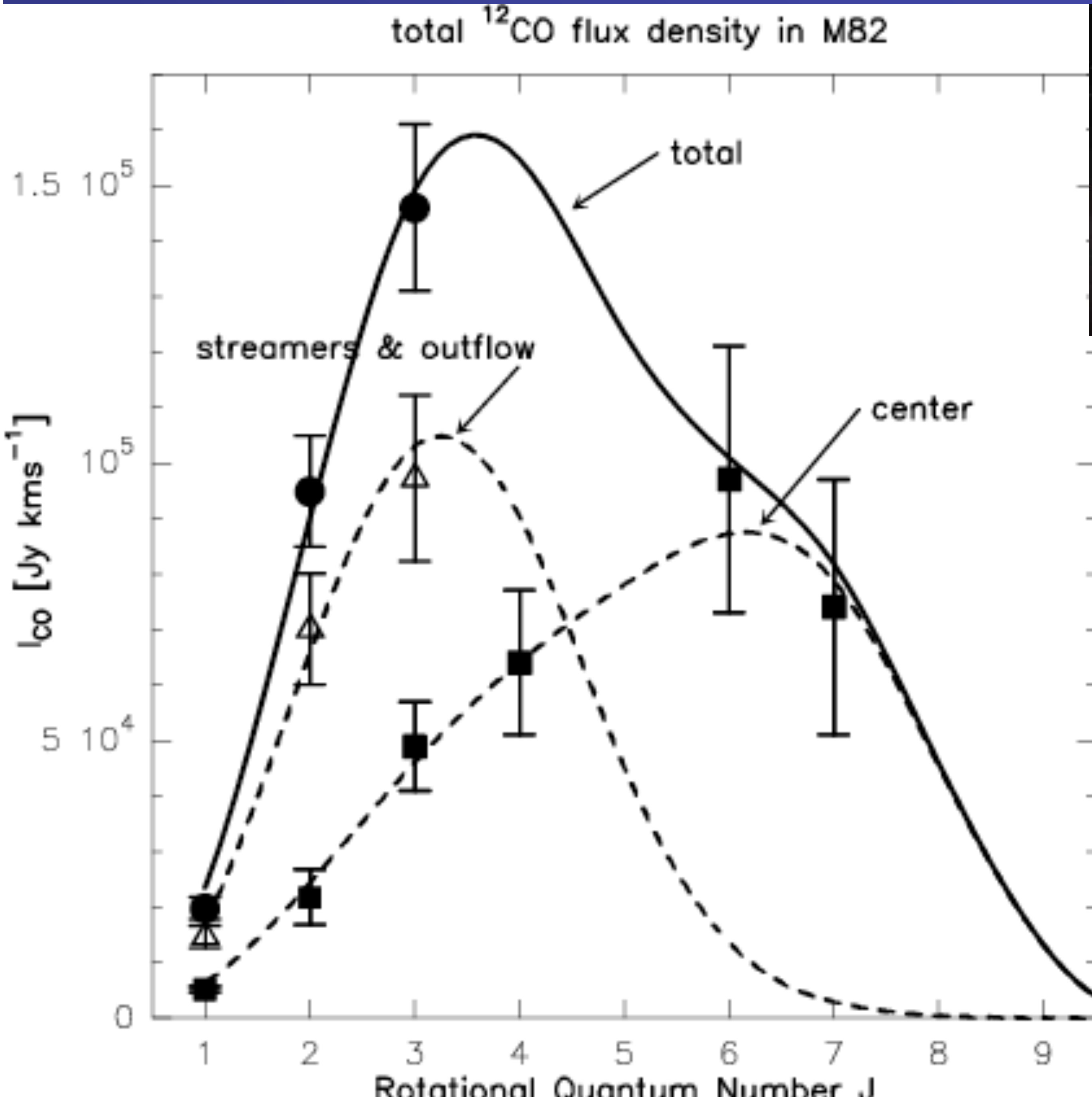

Weiss and Scoville

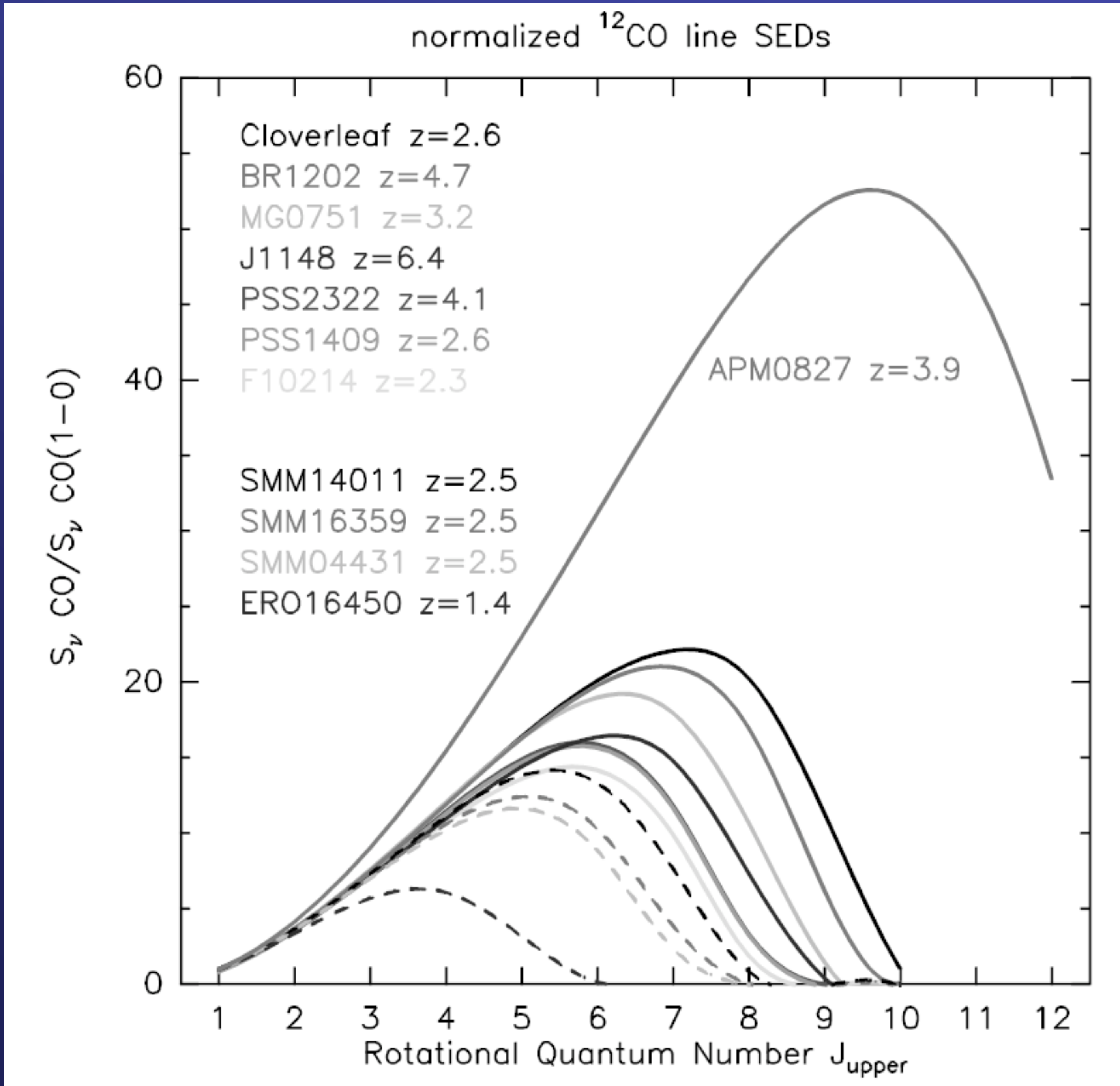

Weiss et al. 2007

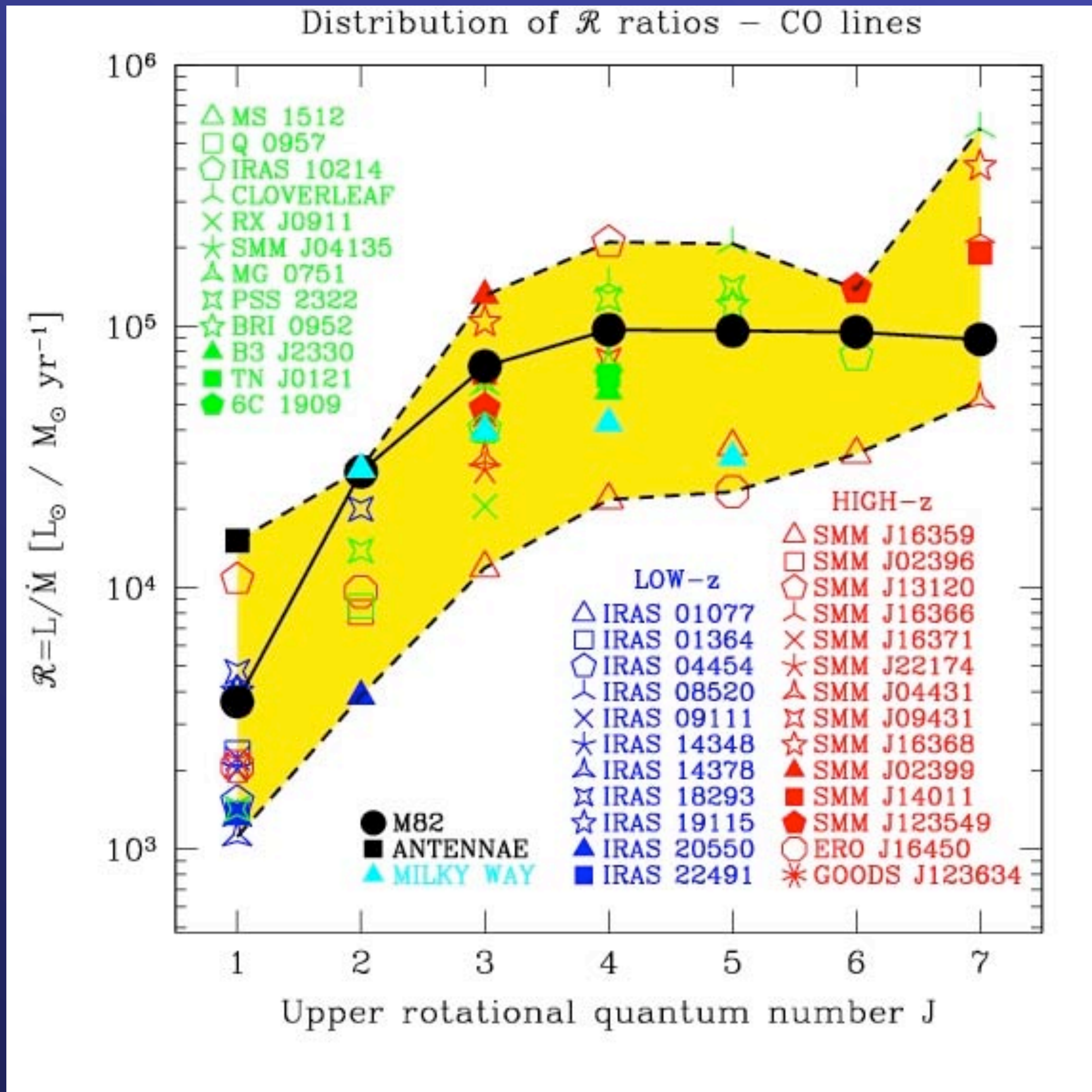

Distribution of ℛ ratios – CO lines
ℛ=L/Ṁ [L⊙ / M⊙ yr⁻¹]
Upper rotational quantum number J
MS 1512
Q 0957
IRAS 10214
CLOVERLEAF
RX J0911
SMM J04135
MG 0751
PSS 2322
BRI 0952
B3 J2330
TN J0121
6C 1909
LOW-z
IRAS 01077
IRAS 01364
IRAS 04454
IRAS 08520
IRAS 09111
IRAS 14348
IRAS 14378
IRAS 18293
IRAS 19115
IRAS 20550
IRAS 22491
HIGH-z
SMM J16359
SMM J02396
SMM J13120
SMM J16366
SMM J16371
SMM J22174
SMM J04431
SMM J09431
SMM J16368
SMM J02399
SMM J14011
SMM J123549
ERO J16450
GOODS J123634
M82
ANTENNAE
MILKY WAY

Motivation

Forthcoming CMB experiments will reach very high angular resolution, probing the high multipole region ($l \sim 10^3$-10^4) of the angular power spectrum

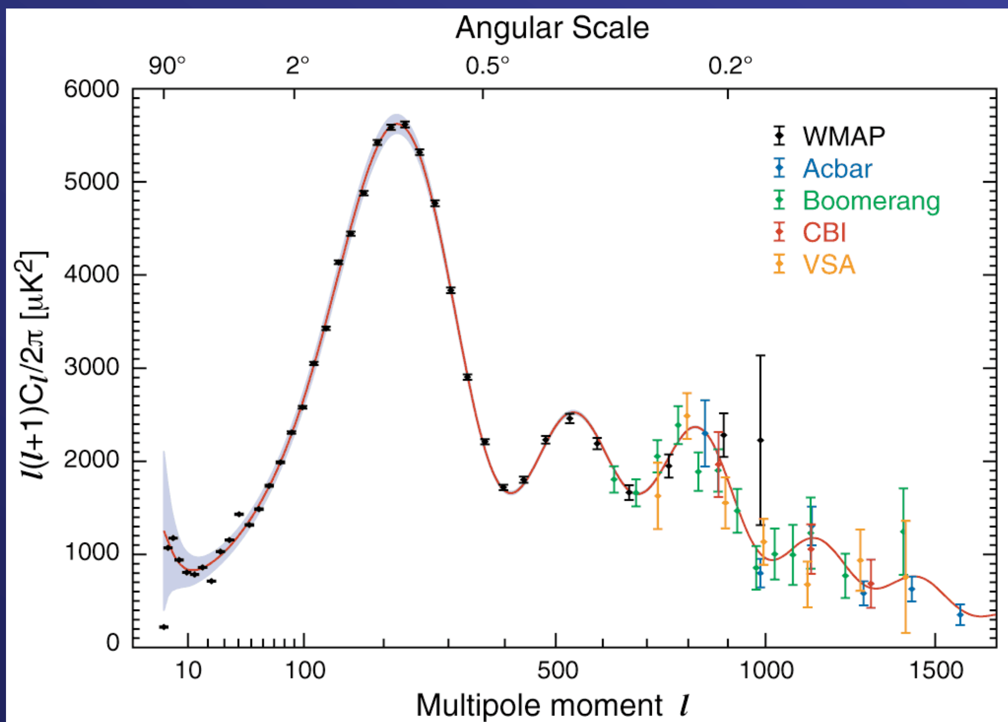

Hinshaw et al. (2007)

SPT

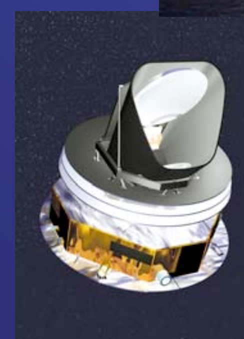

PLANCK

ACT

High frequency channels (150-350 GHz) will be affected by thermal dust emission from star-forming galaxies

Clustering of such sources could be one of the most important foregrounds for these channels

Righi, Hernandez-Monteagudo, Sunyaev, 2008, A&A, 478, 685

CO lines are more important than **dust** as a foreground at low frequencies (15 – 90 GHz):

WMAP, Planck LFI, Quiet and planned modification of CBI

CO line foreground observations require better spectral resolution than WMAP, PLANCK LFI, SPT and ACT have

In principle this is possible

Cosmic Background Imager had 10 spectral channels at 30 GHz

SZ-Array in Owens Valley, California has 145 spectral channeld at 30 GHz

Righi, Hernandez-Monteagudo, Sunyaev, 2008, A&A, 478, 685

Results: power spectra

Two terms: POISSON + CORRELATION

$$\langle \Delta I_\nu(\vec{n}_1)\Delta I_\nu(\vec{n}_2)\rangle = \sum_l \frac{2l+1}{4\pi}\left(C_l^P + C_l^C\right)P_l(\vec{n}_1\cdot\vec{n}_2)$$

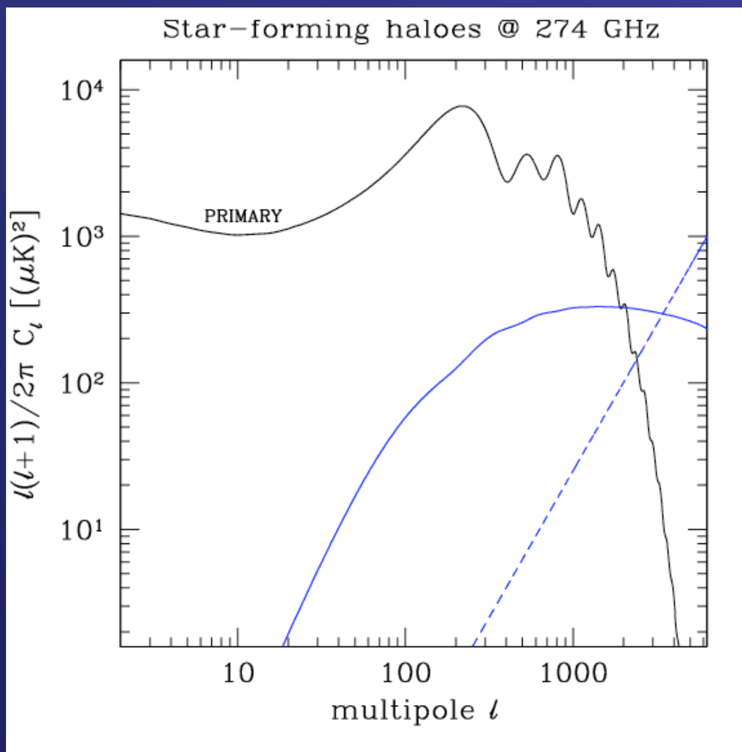

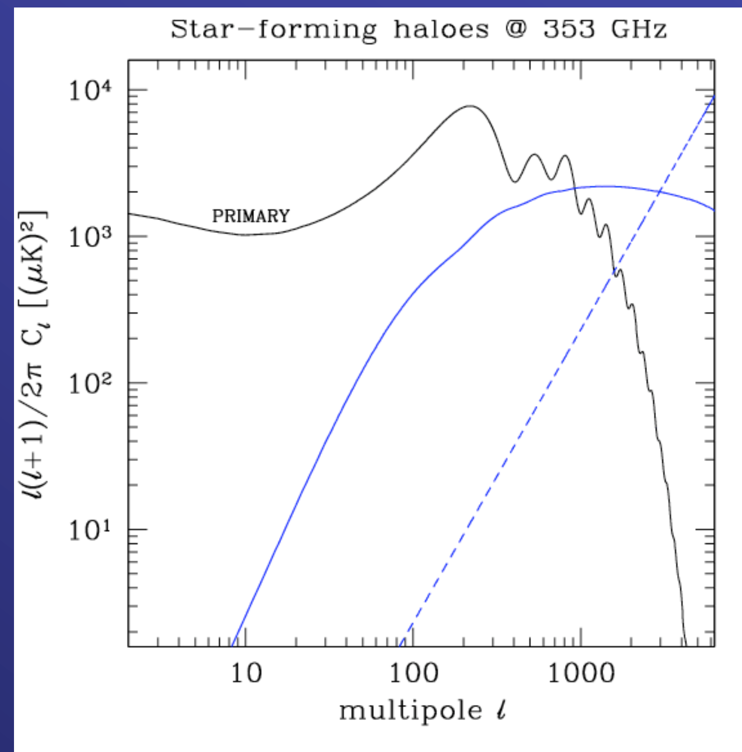

Dust emission will be one of the most important small-scale foregrounds for the high-frequency channels of the future experiments

Good agreement with earlier estimates (Haiman & Knox 00)

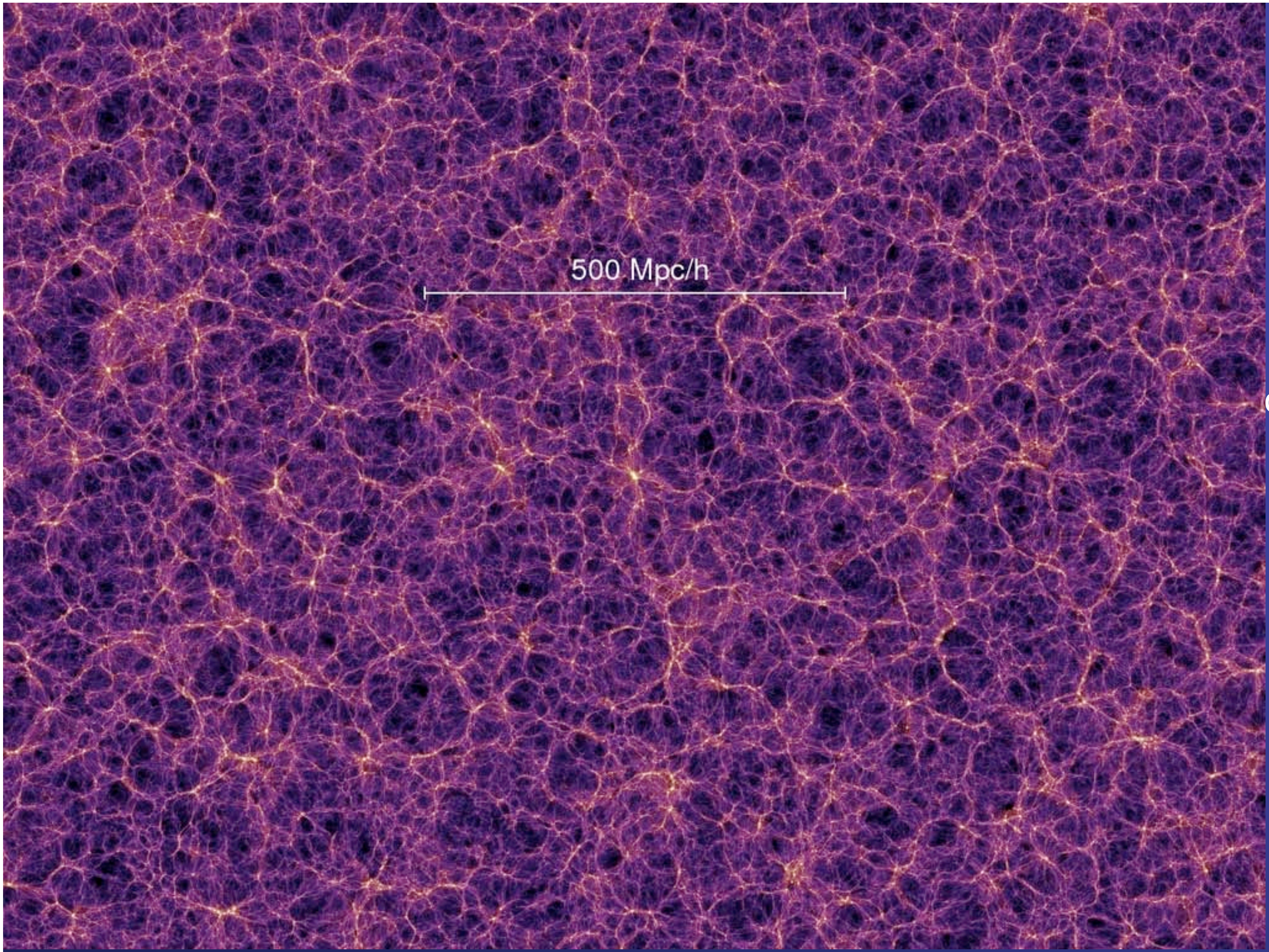

Best Contrast!!!

spectral resolution 10^-3 corresponds to similar dz/z

higher Cl's

This slice through the density field is 15 Mpc/h thick (Volker Springel).

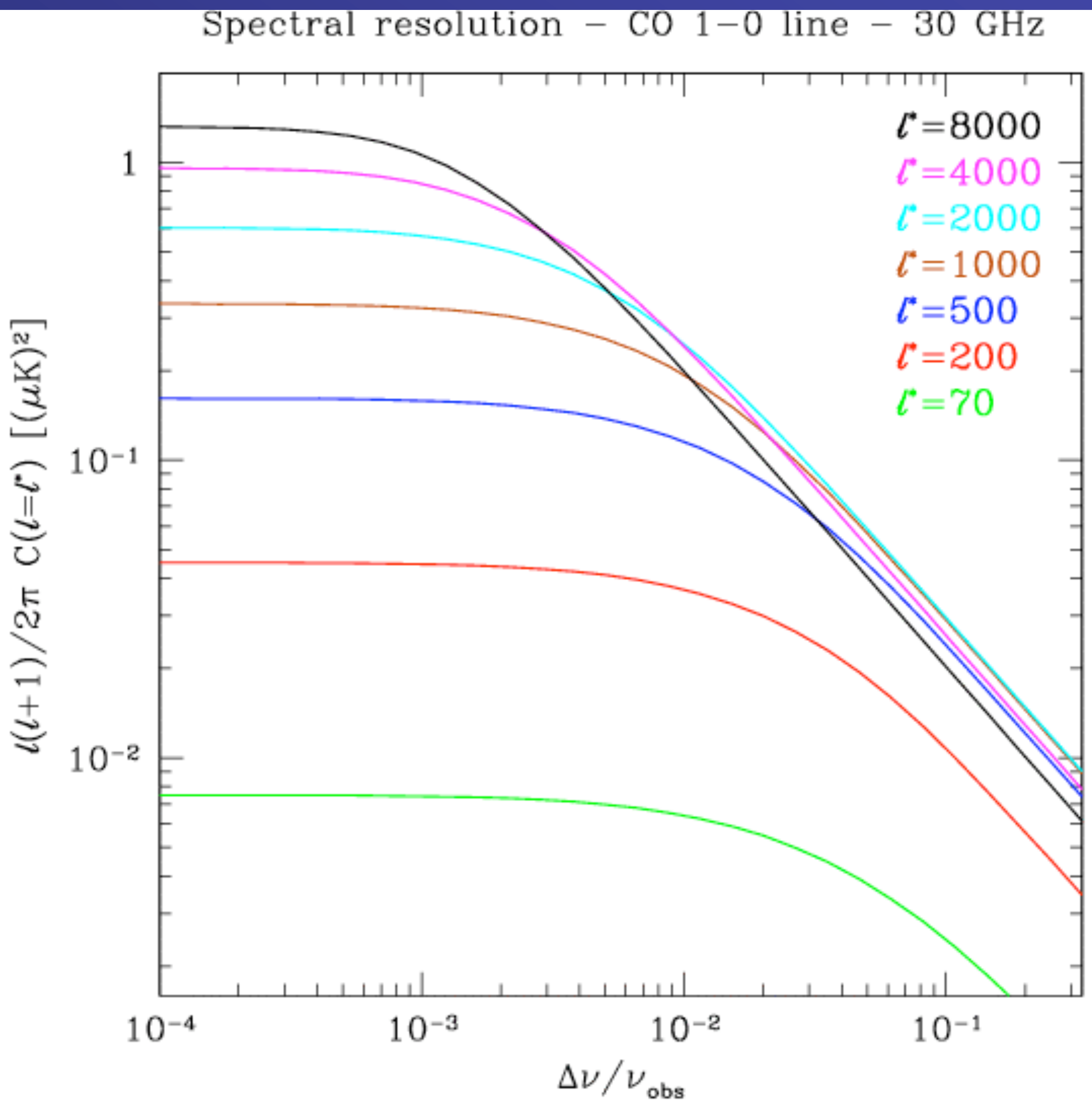

Increase of spectral resolution 300 times provides 100 – 300 times increase in sensitivity of Cl's measurement

But only for high
l > 1000

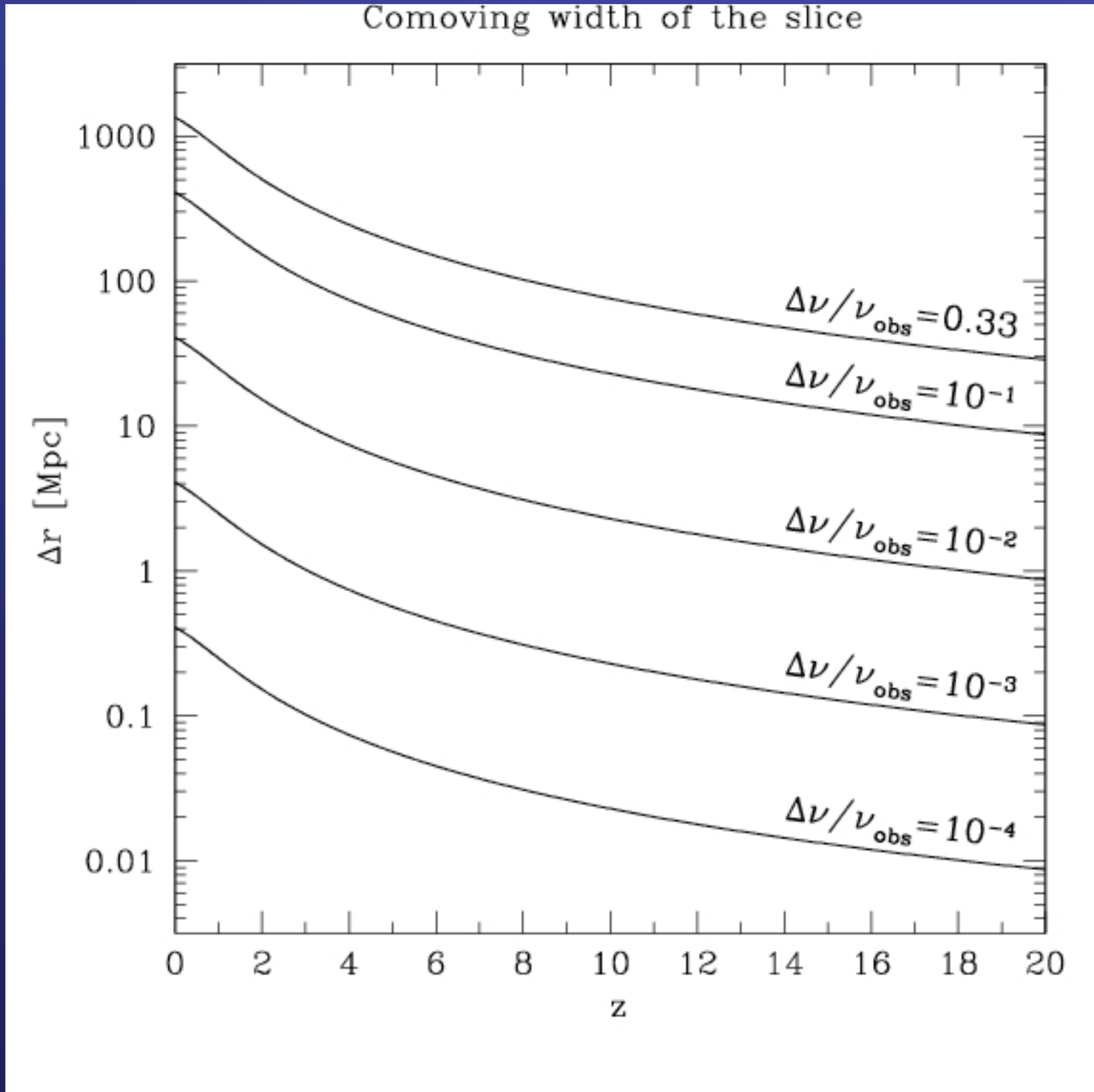

Comoving width of the slice
1000
100
10
1
0.1
0.01
Δr [Mpc]
0
2
4
6
8
10
12
14
16
18
20
z
Δν/ν_obs=0.33
Δν/ν_obs=10^-1
Δν/ν_obs=10^-2
Δν/ν_obs=10^-3
Δν/ν_obs=10^-4

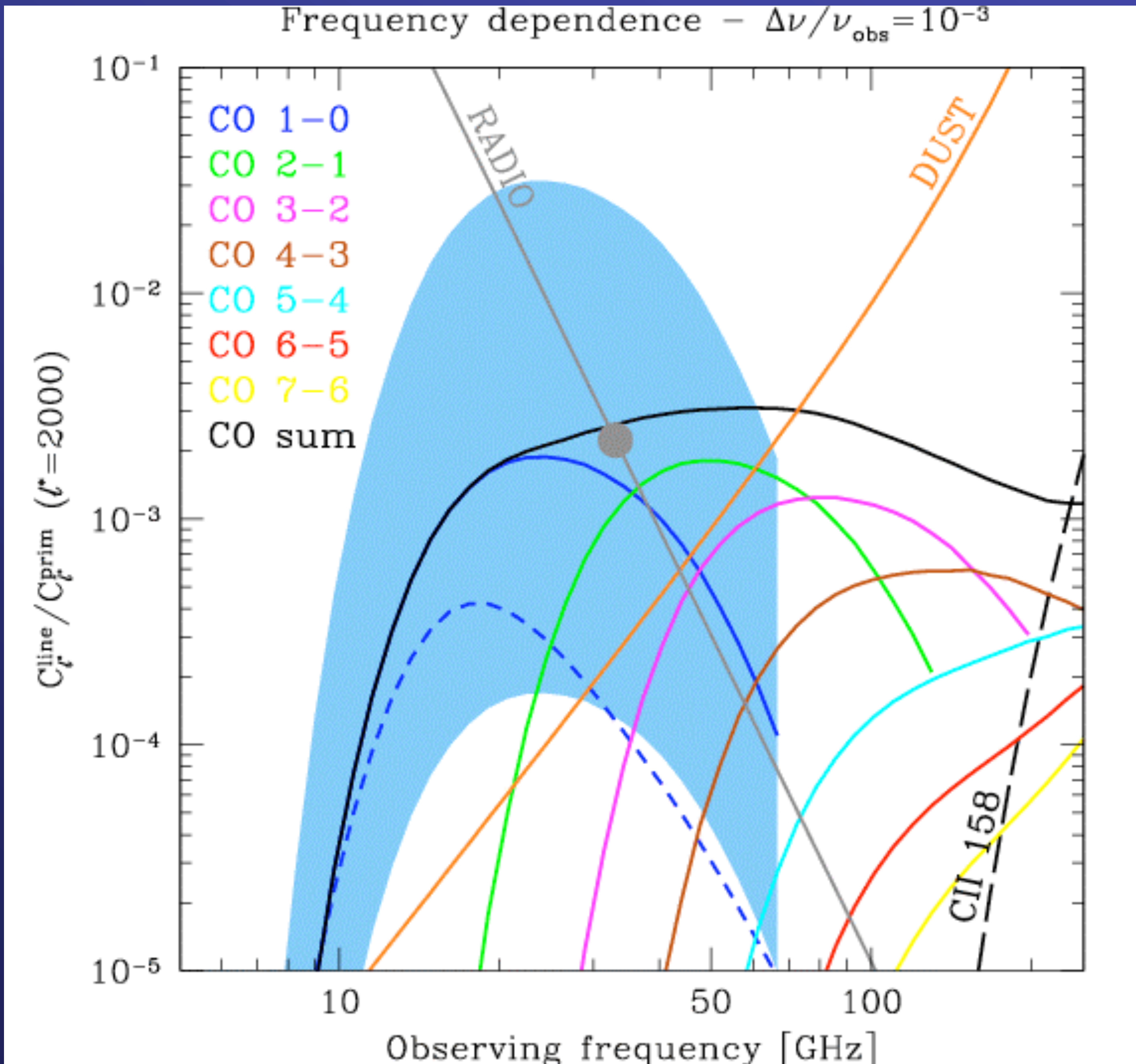

Frequency dependence − $\Delta\nu/\nu_{obs}=10^{-3}$
CO 1−0
CO 2−1
CO 3−2
CO 4−3
CO 5−4
CO 6−5
CO 7−6
CO sum
RADIO
DUST
CII 158
$C_\ell^{line}/C_\ell^{prim}$ (ℓ=2000)
10^{-1}
10^{-2}
10^{-3}
10^{-4}
10^{-5}
10
50
100
Observing frequency [GHz]

Outline

Merging model for star-formation inside haloes

Observational data for CO line emission from merging galaxies

Observational tests and model calibration

Results: power spectra of angular fluctuations

Star formation from mergers

BASIC IDEA (Barkana & Loeb, 2000)

Derive star formation as the rate of accretion of baryonic mass into new haloes

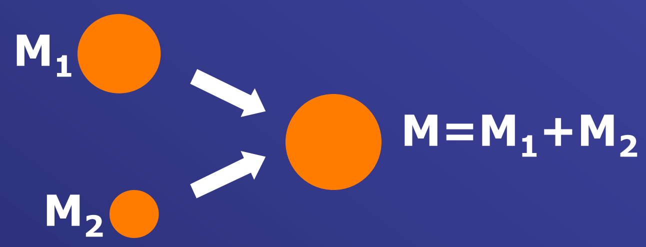

Stellar mass produced in the merger is a function of the merging masses, limited by cooling time

$$M_*^1 = \frac{\Omega_b}{\Omega_m} \eta M_1 \frac{M_2}{M/2} \qquad M_*^2 = \frac{\Omega_b}{\Omega_m} \eta M_2 \frac{M_1}{M/2}$$

For a given cosmological model, rate of merging is derived in the context of the extended-PS theory (Lacey & Cole, 1993)

Future clusters of galaxies and superclusters contained more merging objects

Star formation timescales

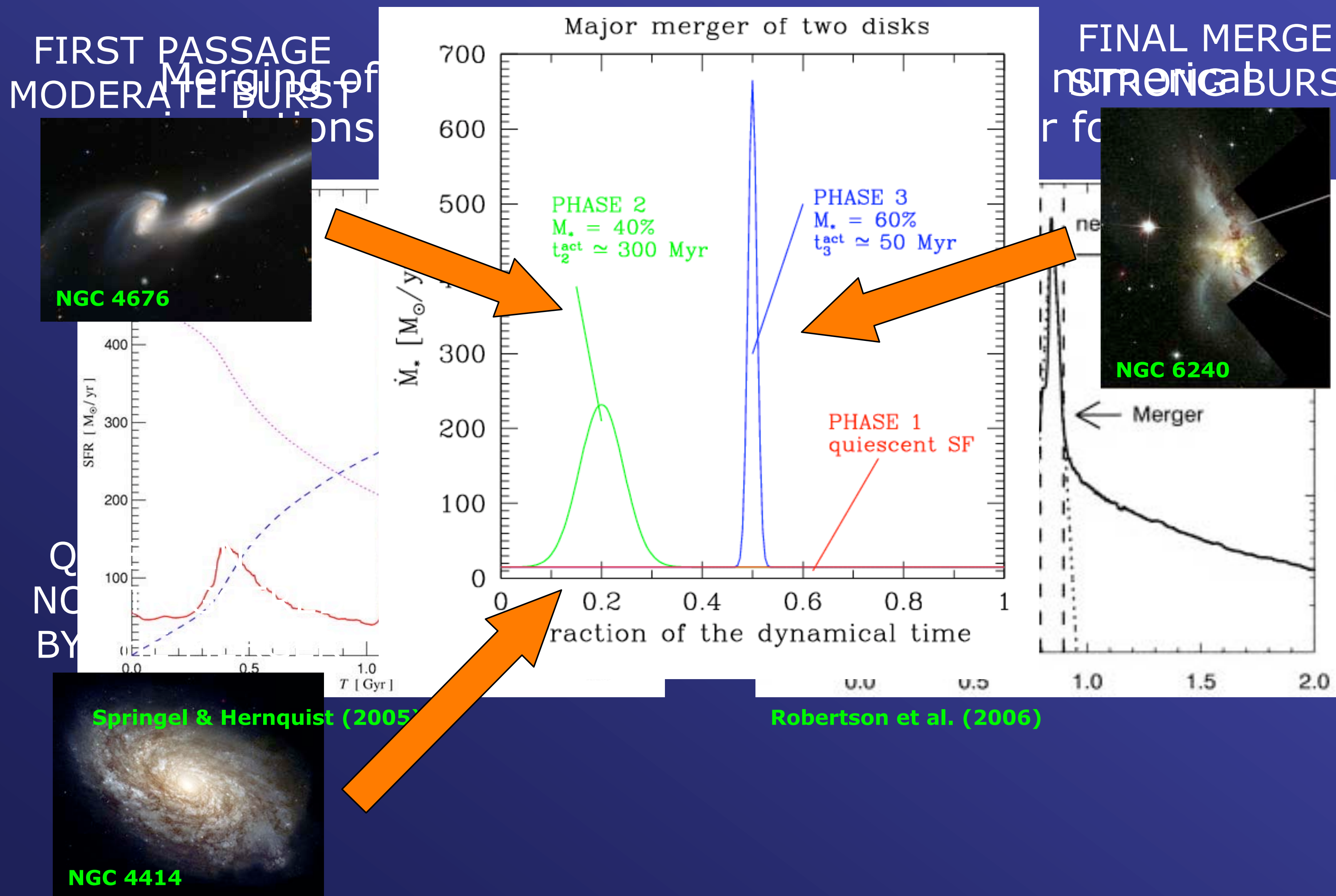

Star formation timescales

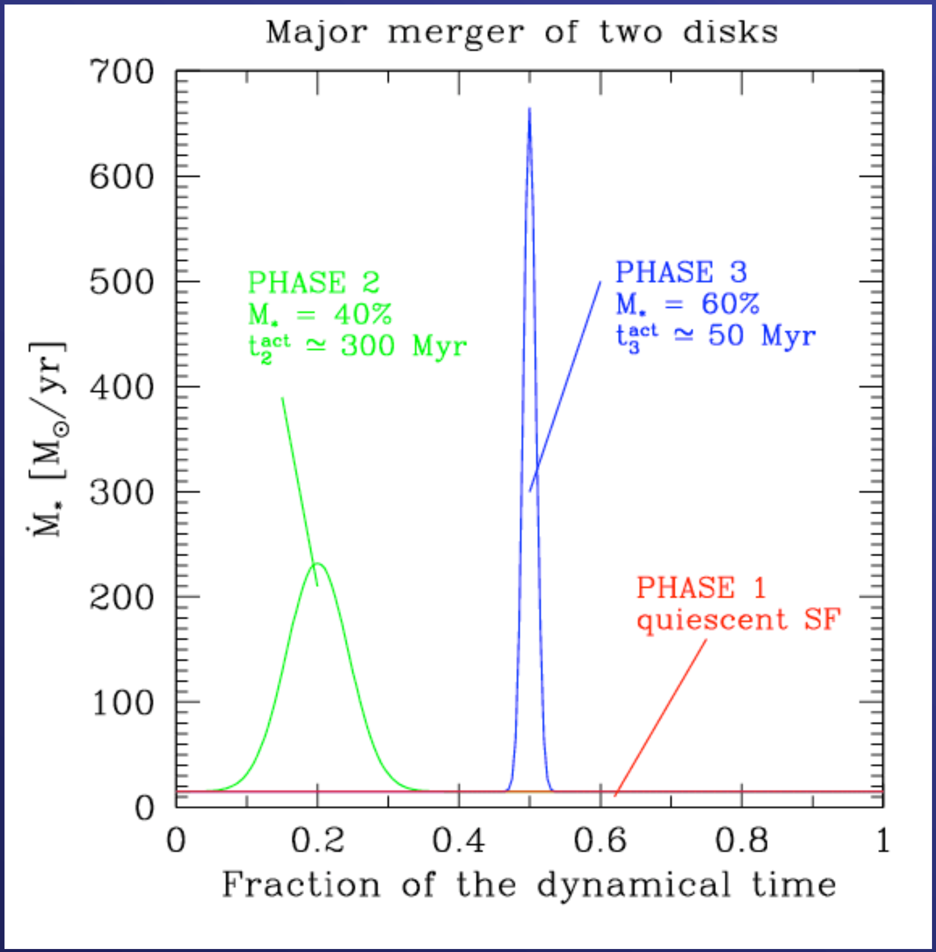

TWO SEPARATE POPULATIONS

40% of M_* is produced during first passage (due to tidal deformation, shocks and gas compression)
$t_{char} \sim 3\times10^8$ years

60% of M_* is produced in the final coalescence (strong burst when the two galaxies finally merge together)
$t_{char} \sim 5\times10^7$ years

Spectral Resolution 10^-3

- DUST/CO(2-1) = 0.005
- DUST/CO(3-2) = 0.009
- DUST/CO(4-3) = 0.020
- DUST/CO(5-4) = 0.054
- DUST/CO(6-5) = 0.122
- DUST/CO(7-6) = 0.236

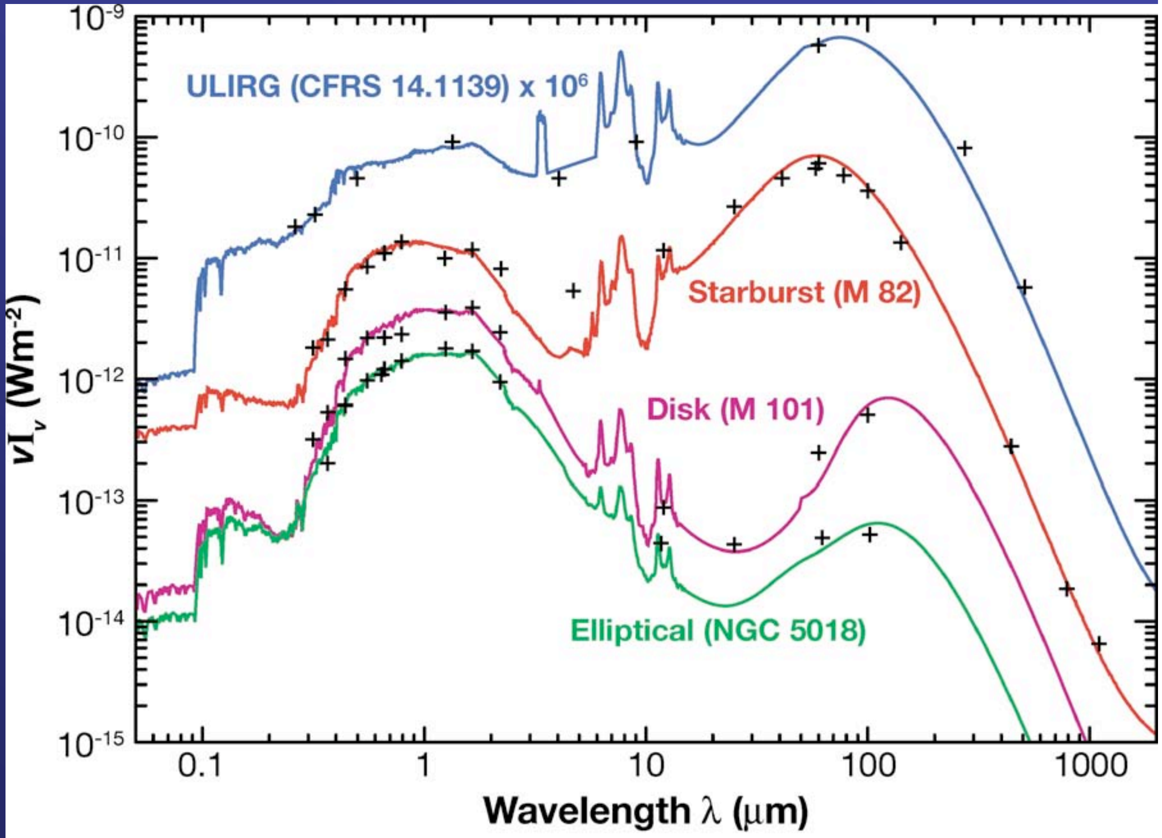

Lagache, G et al. 2005
Annu. Rev. Astron. Astrophys. 43: 727–68

Model summary

MERGING MODEL
Prescription for star formation in major mergers

$L_{line} = \mathcal{R}\,SFR$

Line luminosity: assumed linear scaling with star formation rate

+

OBSERVATIONAL DATA
to calibrate the proportionality ($\mathcal{R}$ ratio): M82, Antennae, Milky Way, low-z IRAS galaxies, high-z sub-mm galaxies, QSO, LBGs, radio galaxies

=

$\mathcal{R}$ ratio for CO transition (J+1=1-7) and atomic species (CII, NII, OI…)

RESULTS
Angular power spectra
Spectral resolution dependence
Frequency dependence
Foregrounds comparison

Cosmic star-formation rate

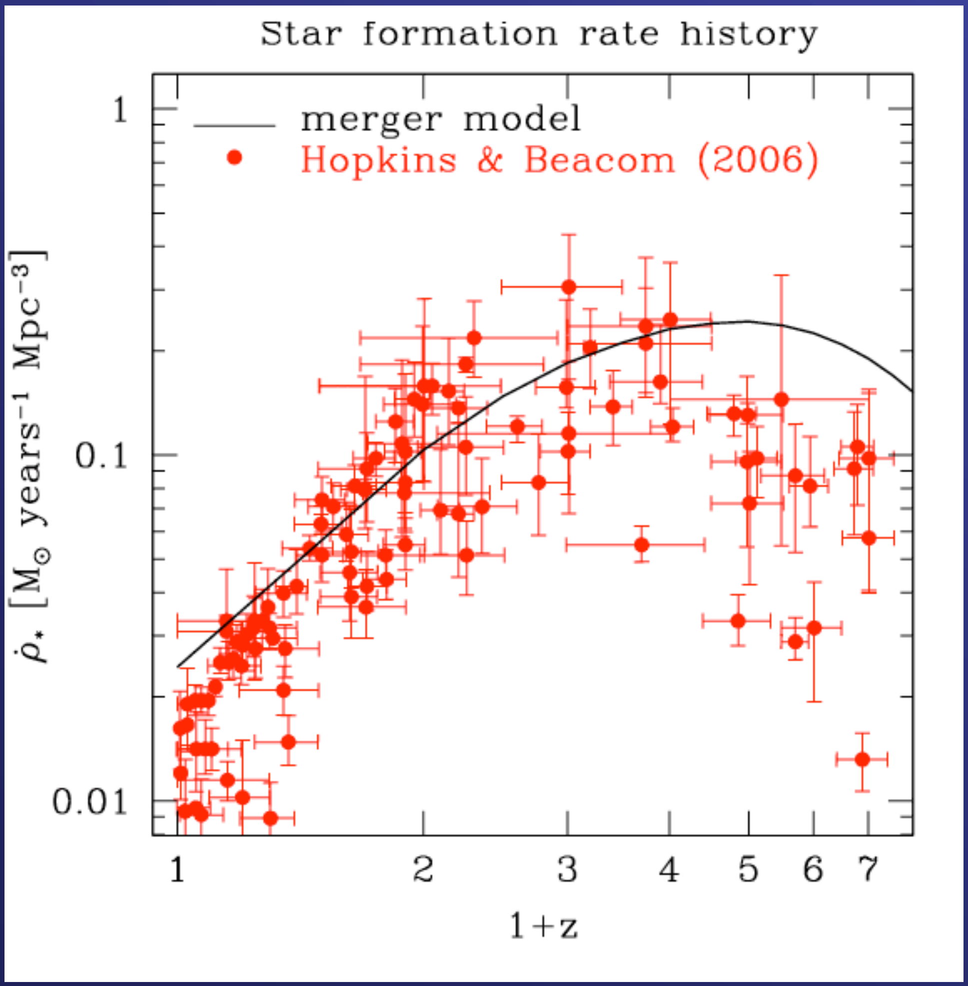

The star formation model can be compared with observations by computing cosmic SFR (Madau plot)

$$\dot{\rho}_*(z) = \int dM_1 \int dM \frac{dN_{merg}}{dMdt} \frac{dn}{dM_1} M_*(M_1, M_2, z)$$

Rather good agreement is obtained with a star formation efficiency $\eta = 5\%$

OBSERVATIONAL SAMPLE

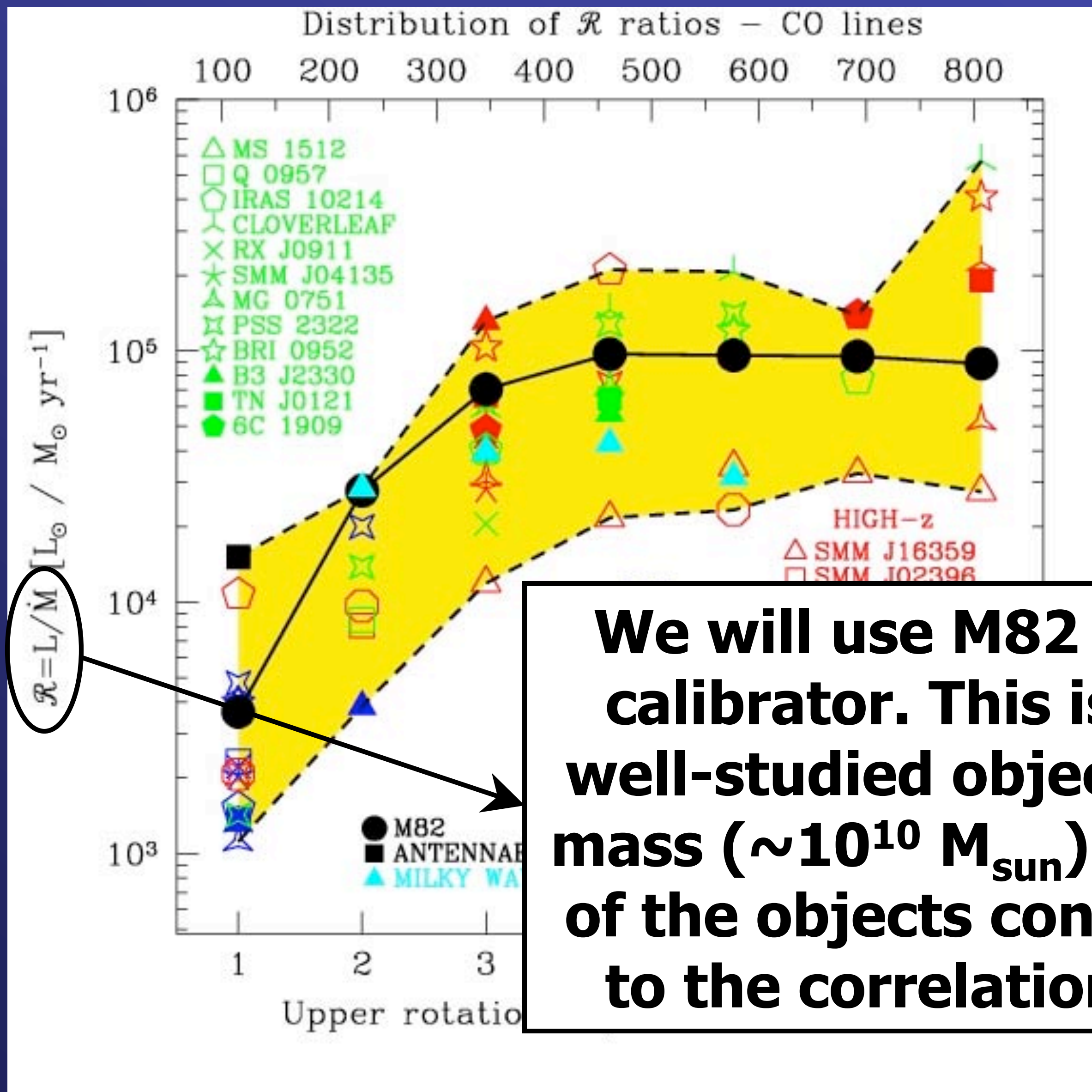

We will use M82 as main calibrator. This is a very well-studied object and its mass (~10^{10} M_{sun}) is typical of the objects contributing to the correlation signal

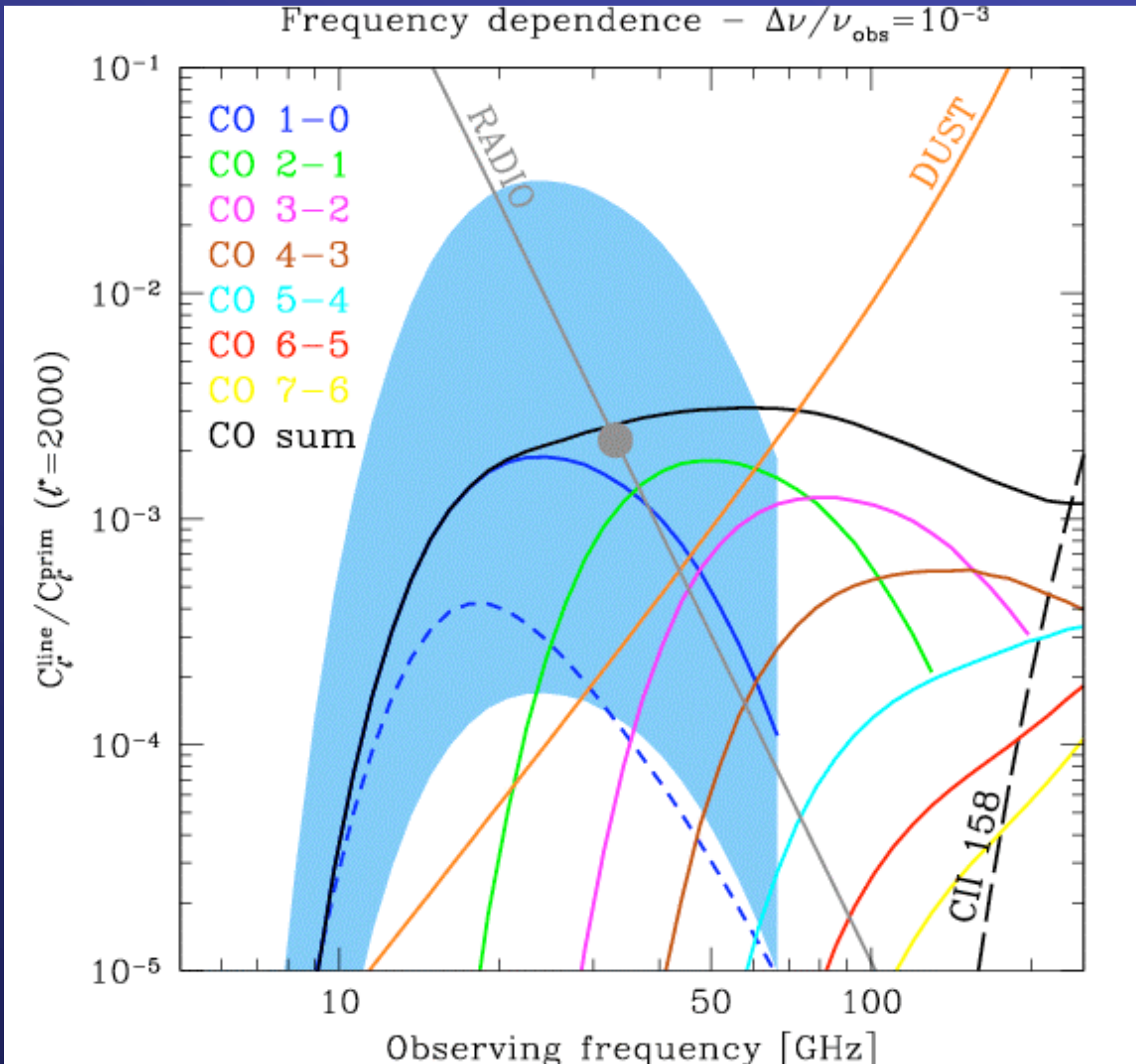

Frequency dependence – $\Delta\nu/\nu_{obs}=10^{-3}$
CO 1−0
CO 2−1
CO 3−2
CO 4−3
CO 5−4
CO 6−5
CO 7−6
CO sum
RADIO
DUST
CII 158
10^{-1}
10^{-2}
10^{-3}
10^{-4}
10^{-5}
10
50
100
Observing frequency [GHz]
$C_\ell^{line}/C_\ell^{prim}$ (ℓ=2000)

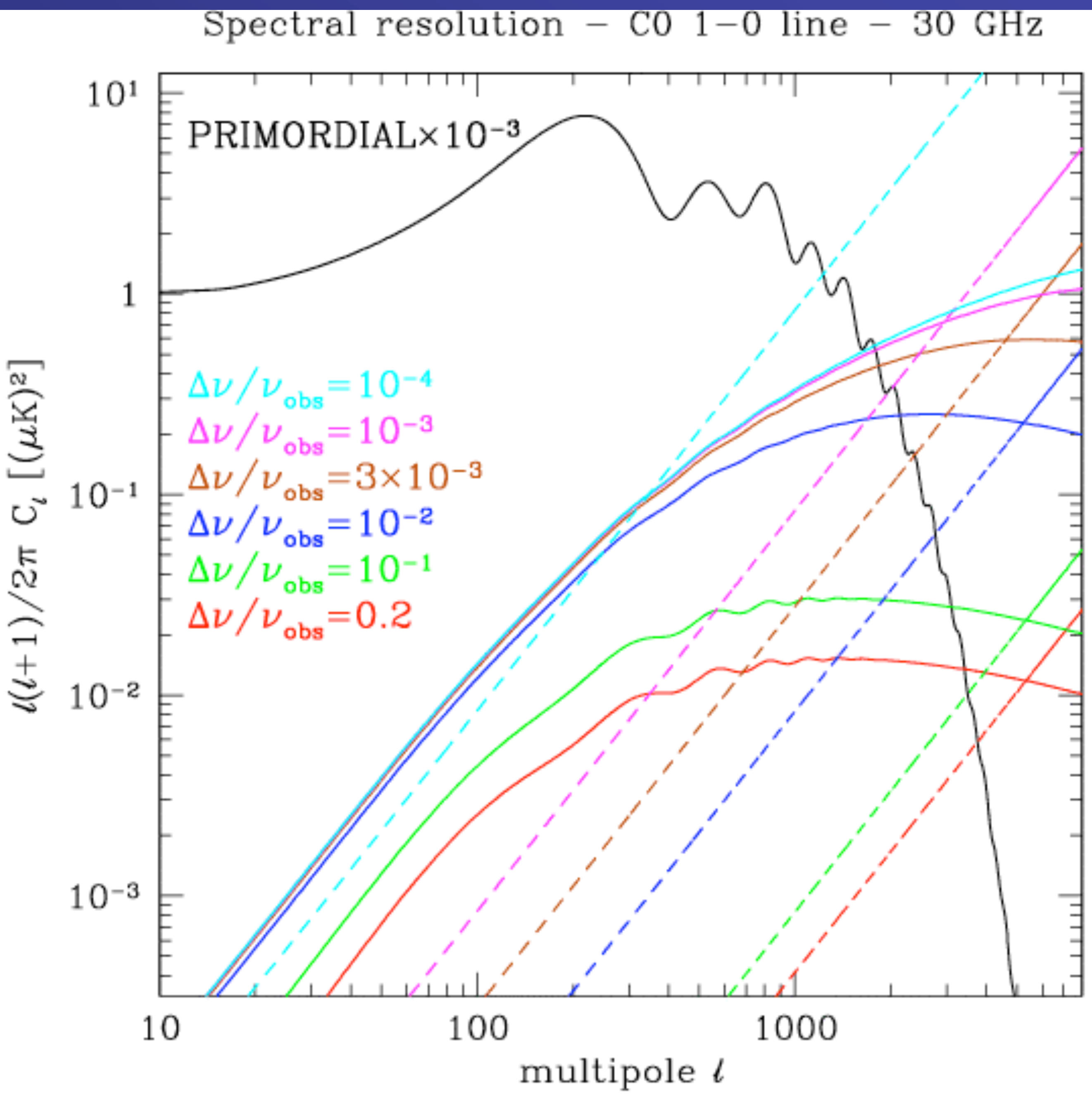

Correlated contribution (solid curves)

Poisson contribution (dashed lines) behaves differently

too high spectral resolution is useless for correlated contribution

CORRELATION TERM

Stars are formed in highly clustered overdense regions.
The correlation (or clustering) term accounts for this

It depends on the halo number density **squared**.
On the other hand, the Poisson term is linear with the density.

For large number densities (not too rare objects) the clustering term will dominate over the Poisson

Conclusions

1. It is possible to separate CO contribution to CI’s from dust

2. The way to measure the rate of C and O production in early Universe

3. To measure sigma-8

4. To follow star formation rate in the Universe

Righi, M.; Hernández-Monteagudo, C., Sunyaev, R. A., 2008
Astronomy and Astrophysics, 489, pp.489-504

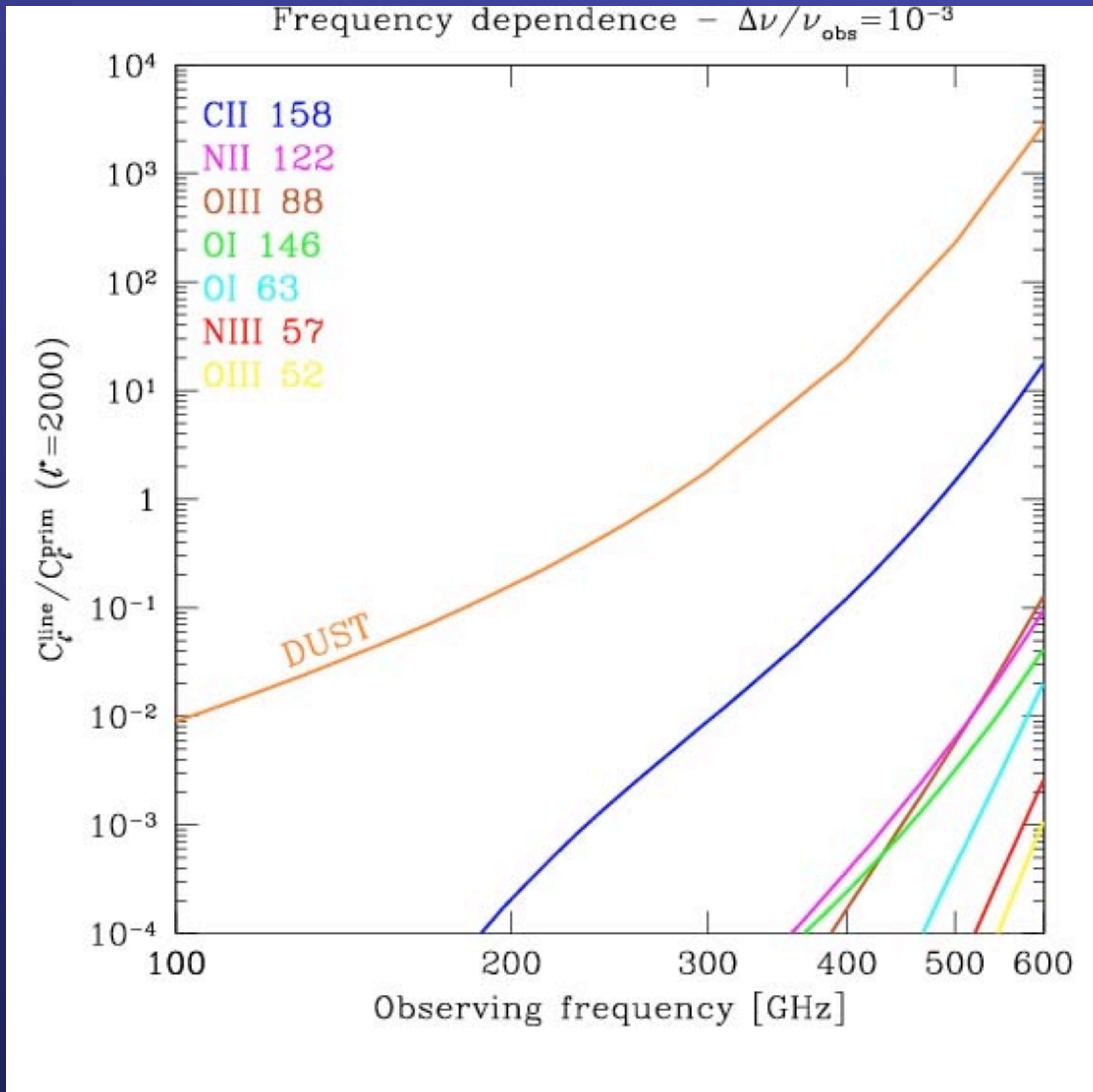

Frequency dependence − Δν/ν_obs=10^−3
CII 158
NII 122
OIII 88
OI 146
OI 63
NIII 57
OIII 52
DUST
C_ℓ^line/C_ℓ^prim (ℓ=2000)
10^4
10^3
10^2
10^1
1
10^−1
10^−2
10^−3
10^−4
100
200
300
400
500
600
Observing frequency [GHz]

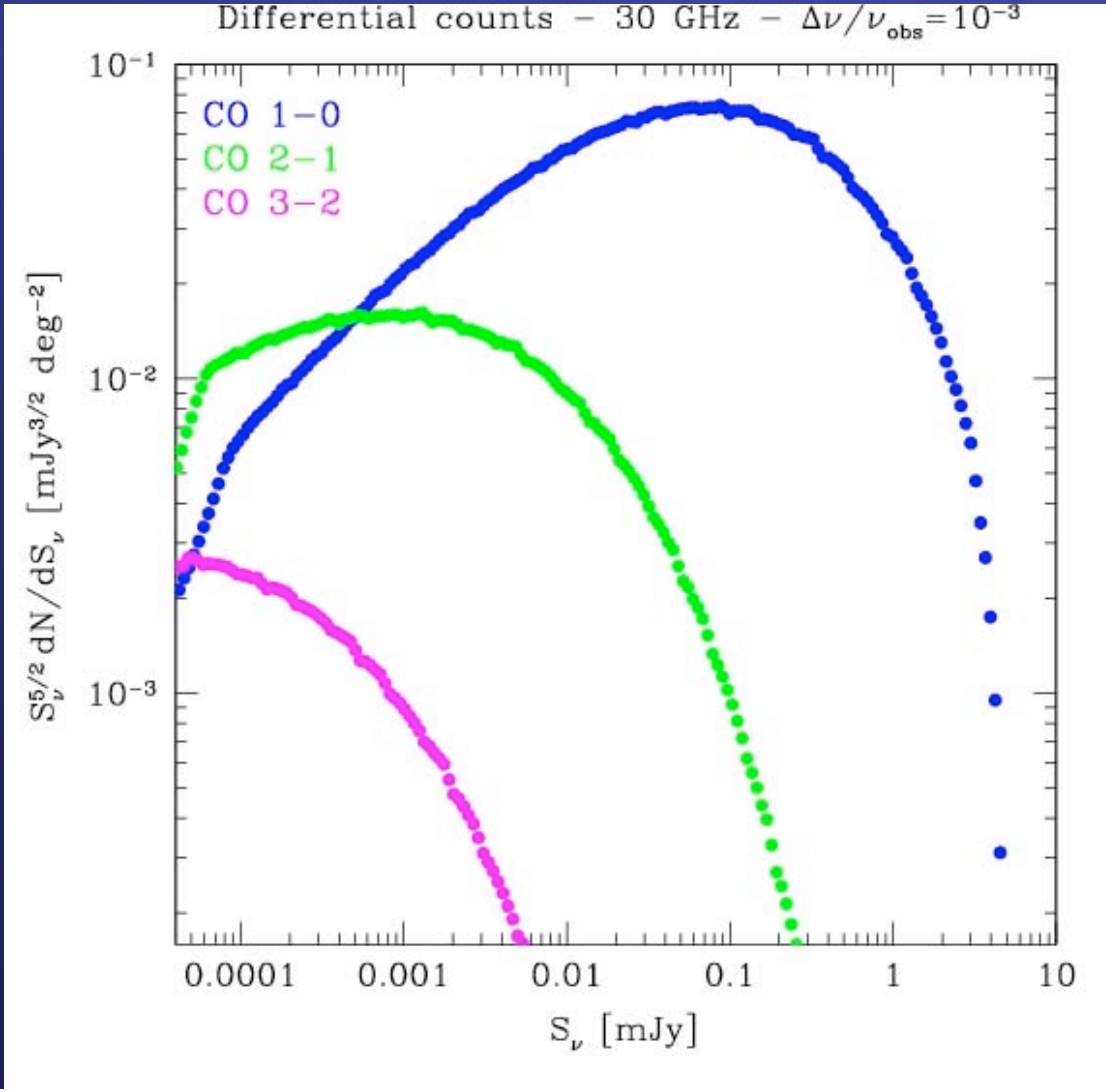
Differential counts - 30 GHz - Δν/ν_obs=10^-3
CO 1-0
CO 2-1
CO 3-2
10^-1
10^-2
10^-3
S_ν^5/2 dN/dS_ν [mJy^3/2 deg^-2]
0.0001
0.001
0.01
0.1
1
10
S_ν [mJy]

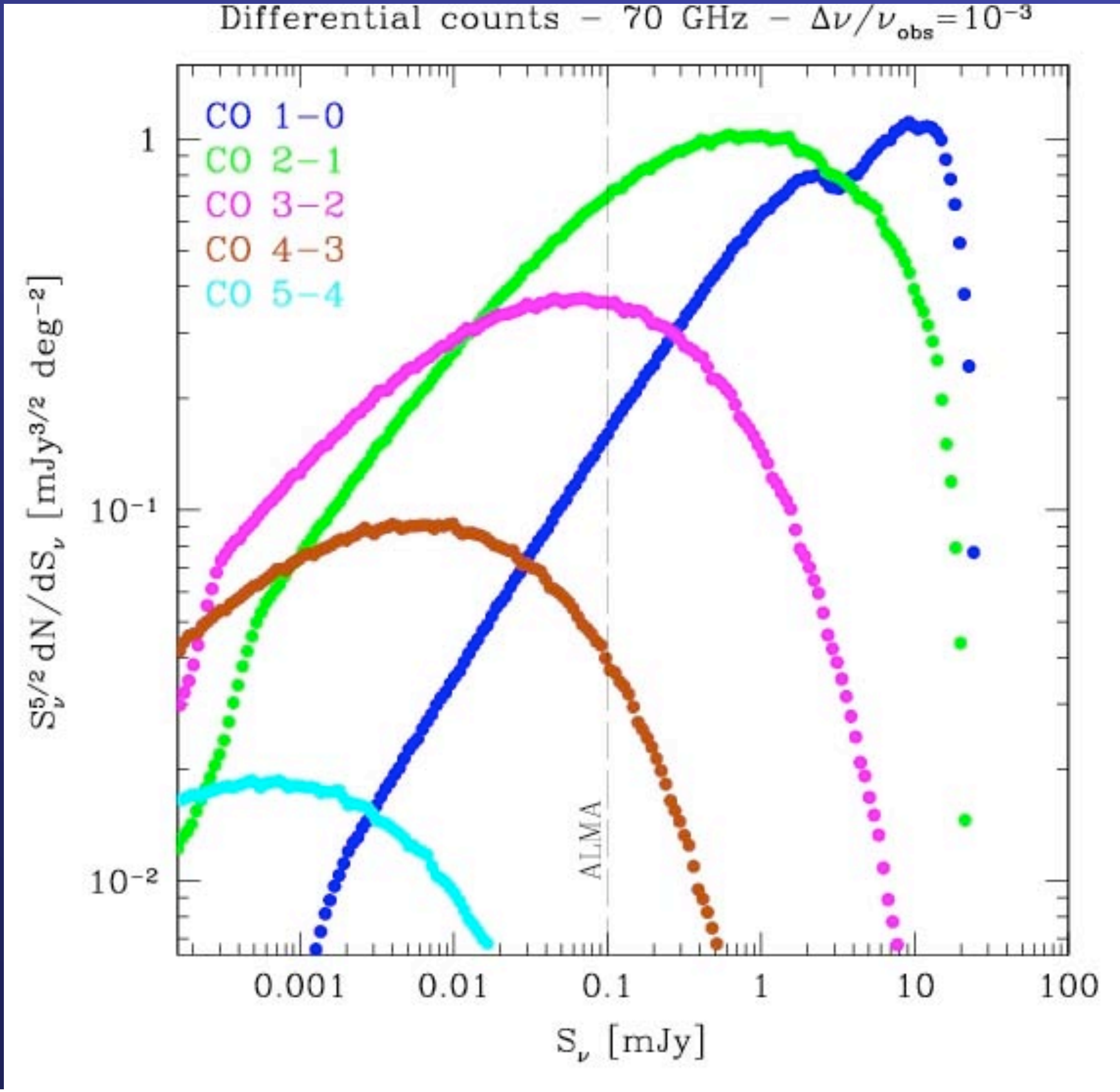

Differential counts – 70 GHz – $\Delta\nu/\nu_{obs}=10^{-3}$
CO 1–0
CO 2–1
CO 3–2
CO 4–3
CO 5–4
ALMA
$S_\nu^{5/2}\,dN/dS_\nu$ [mJy$^{3/2}$ deg^{-2}]
S_ν [mJy]
1
10^{-1}
10^{-2}
0.001
0.01
0.1
1
10
100

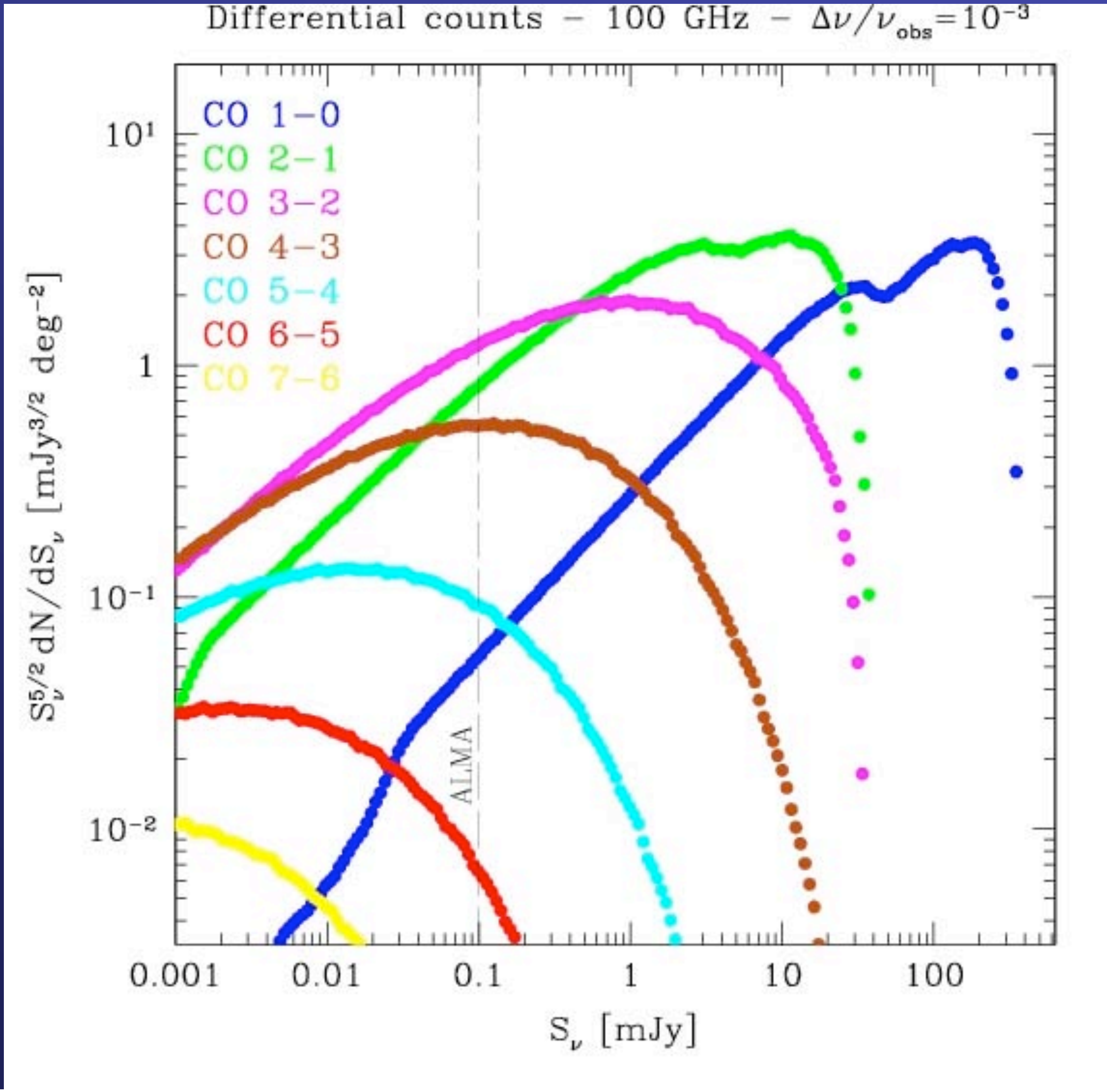
Differential counts – 100 GHz – $\Delta\nu/\nu_{obs}=10^{-3}$
CO 1−0
CO 2−1
CO 3−2
CO 4−3
CO 5−4
CO 6−5
CO 7−6
ALMA
$S_\nu^{5/2}\,dN/dS_\nu$ [$mJy^{3/2}\ deg^{-2}$]
10^1
1
10^{-1}
10^{-2}
0.001
0.01
0.1
1
10
100
S_ν [mJy]

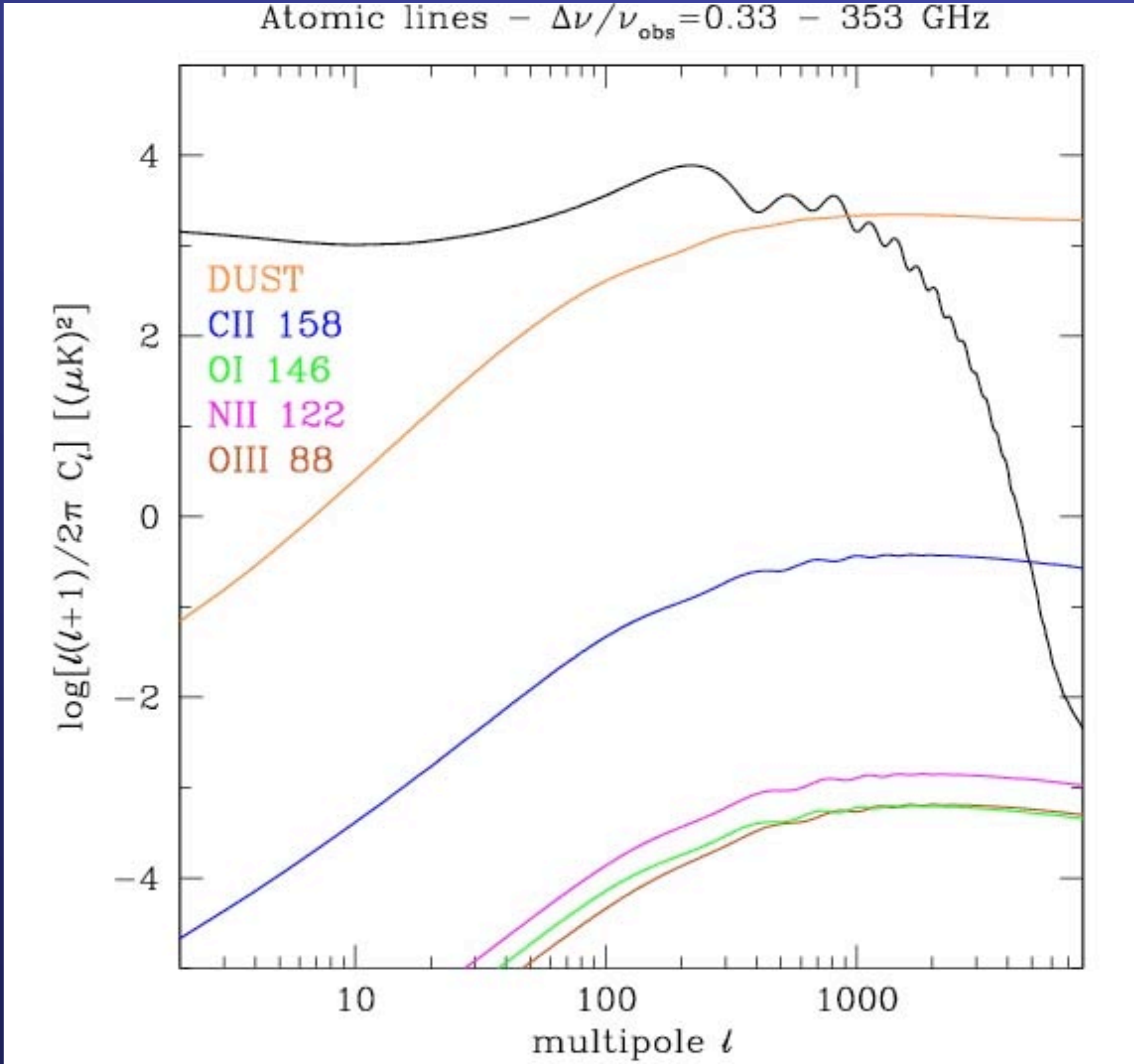

There is a possibility to increase Cl's for the lines 100 times Increasing spectral resolution

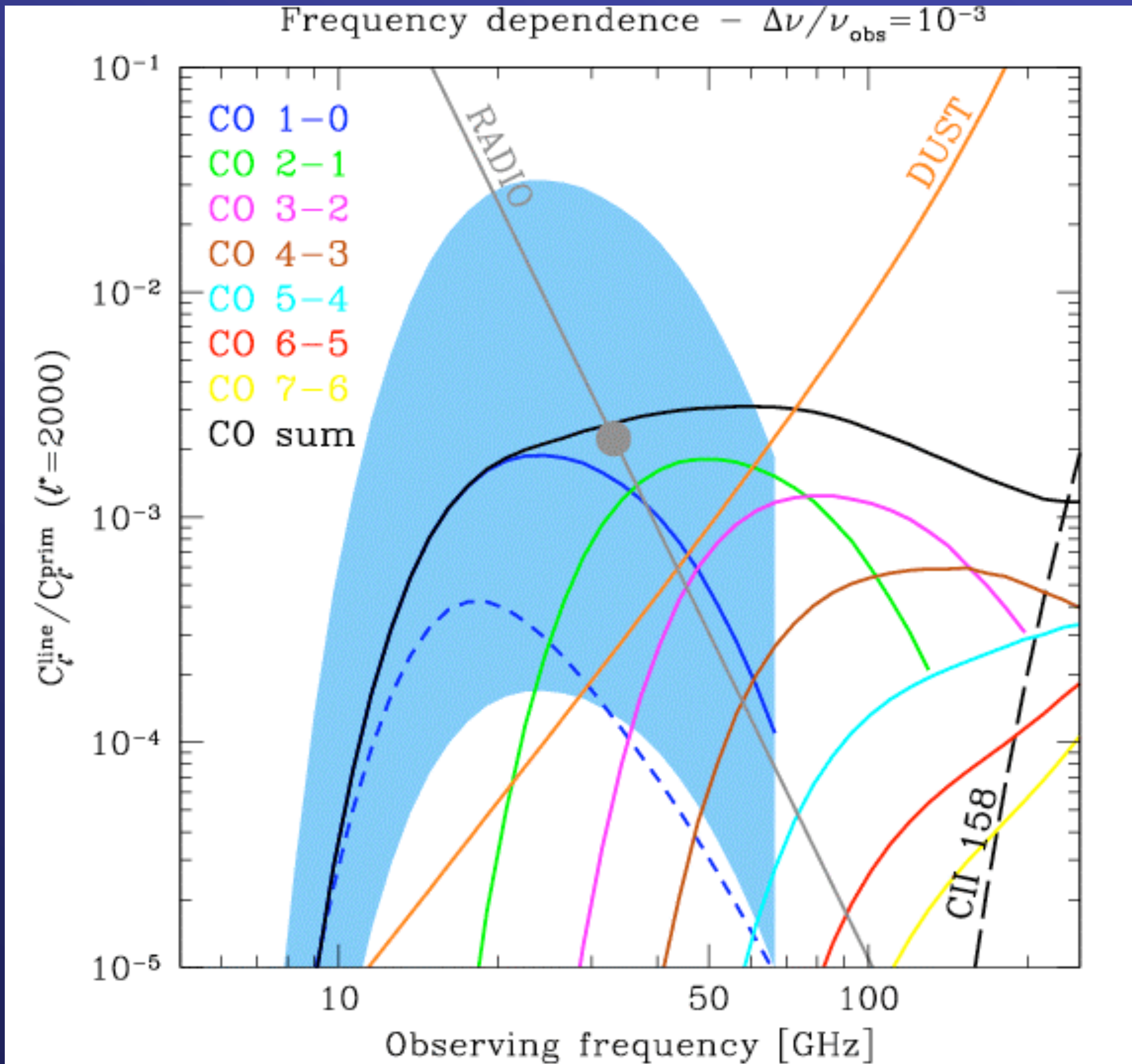

Frequency dependence – Δν/ν_obs=10^-3
CO 1−0
CO 2−1
CO 3−2
CO 4−3
CO 5−4
CO 6−5
CO 7−6
CO sum
RADIO
DUST
CII 158
10^-1
10^-2
10^-3
10^-4
10^-5
10
50
100
Observing frequency [GHz]
C_ℓ^line/C_ℓ^prim (ℓ=2000)

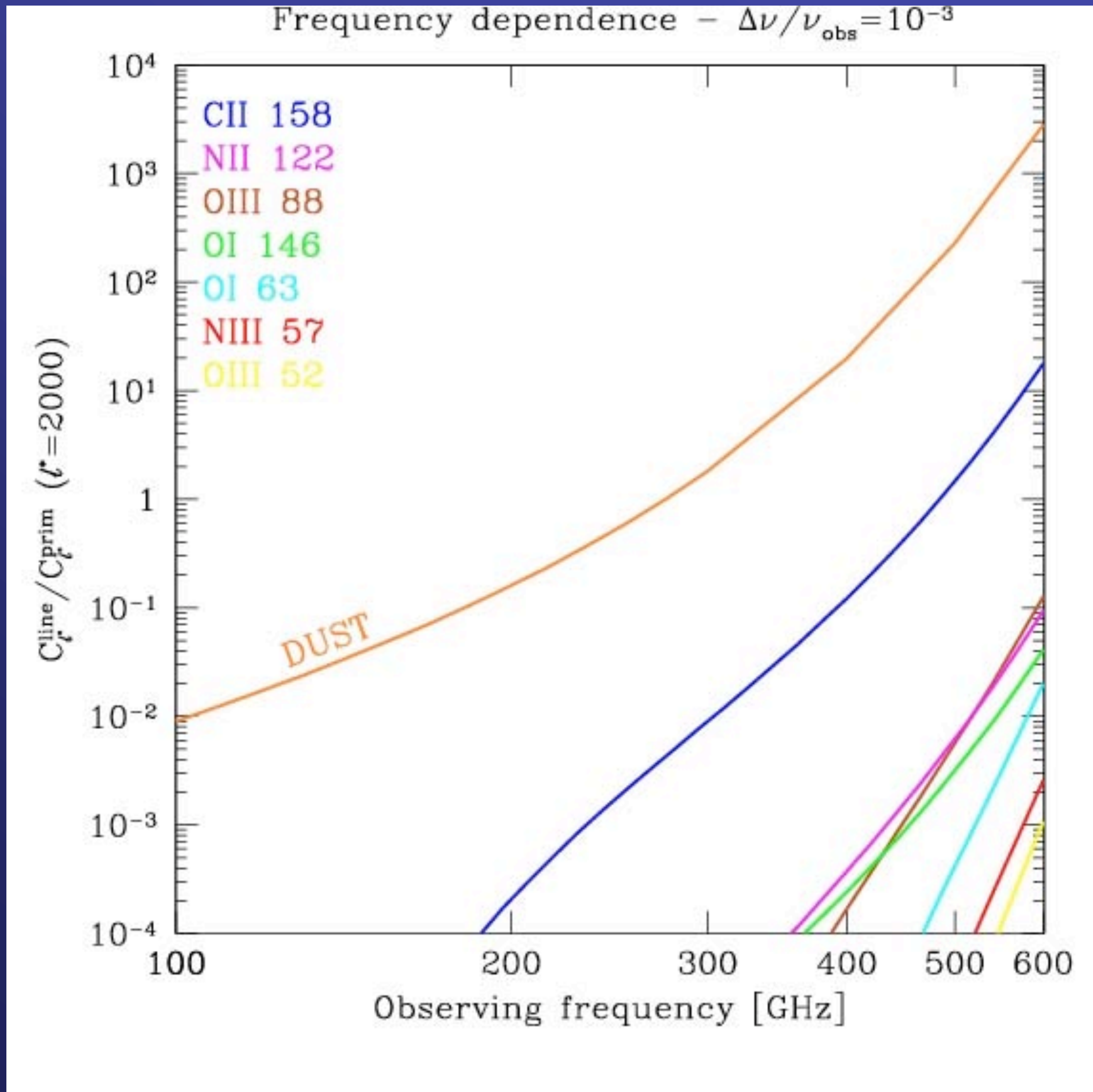

Frequency dependence – $\Delta\nu/\nu_{obs}=10^{-3}$
CII 158
NII 122
OIII 88
OI 146
OI 63
NIII 57
OIII 52
DUST
$C_\ell^{line}/C_\ell^{prim}$ (ℓ=2000)
10^4
10^3
10^2
10^1
1
10^{-1}
10^{-2}
10^{-3}
10^{-4}
100
200
300
400
500
600
Observing frequency [GHz]

"The EPS theory represents the only fully analytic model of the hierarchical growth of structure. While its derivation requires making several gross approximations and assumptions (Bond et al. 1991; Lacey & Cole 1993), it is remarkable that it captures well the qualitative dependences of progenitor mass distributions on redshift and final halo mass and of final halo mass distributions on initial progenitor mass and redshift. However, its accuracy is not sufficient for the present era of precision cosmology. For example, at high redshift, $z = 4$, it can underestimate the typical progenitor mass by factors of 3 or 4, or equivalently the abundance of the most massive progenitors by factors of a few."

Cole et al. 2008

POWER SPECTRUM OF THE FLUCTUTATIONS

Two terms: POISSON + CORRELATION

$$\left\langle \Delta I_\nu(\vec{n}_1)\Delta I_\nu(\vec{n}_2)\right\rangle = \sum_l \frac{2l+1}{4\pi}\left(C_l^P + C_l^C\right)P_l(\vec{n}_1\cdot\vec{n}_2)$$

Generated by the brightest and rare sources

Generated by the most abundant and less bright sources: probes the clustering

CORRELATION TERM

$$C_l^C = \frac{2}{\pi}\int k^2 dk P(k) \left|\Delta_l(k)\right|^2$$

Matter power spectrum

Transfer function: contains l dependence and line profile φ

$$\Delta_l(k) = \int dr j_l(kr)\varphi(r)\left[S(r)\delta_k\right]$$

Source function: contains information about the population

$$S(r) = \int dL_{\nu(1+z)} \frac{dn}{dL_{\nu(1+z)}} \frac{L_{\nu(1+z)}}{4\pi} cH^{-1}(z) b(M,z)$$

Bias factor => clustering

POISSON TERM

$$C_l^P = \left[r^2 \frac{\Delta\nu}{\nu_{obs}} \right]^{-1} \times \int dL_{\nu(1+z)} c H^{-1}(z) \left(\frac{L_{\nu(1+z)}}{4\pi} \right)^2 \frac{d\bar{n}}{dL_{\nu(1+z)}}$$

Linear dependence on the spectral resolution

Proportional to the number of sources

$$\frac{C_l^P}{C_l^C} \propto \frac{nL^2}{(nL)^2} = \frac{1}{n}$$

Poisson power is dominated by rarest (brightest) sources!

The fluctuations below the scale probed by the given $\Delta\nu/\nu_{obs}$ (along the line of sight) are "smeared out".

$$C_l^C \propto \int_0^{k_z^{MAX}} \frac{dk_z}{2\pi} P(k_\perp, k_z) \left|W(k_z)\right|^2$$

The effect of the window function *W* is to change the upper limit of integration to a maximum *k* (minimum scale).

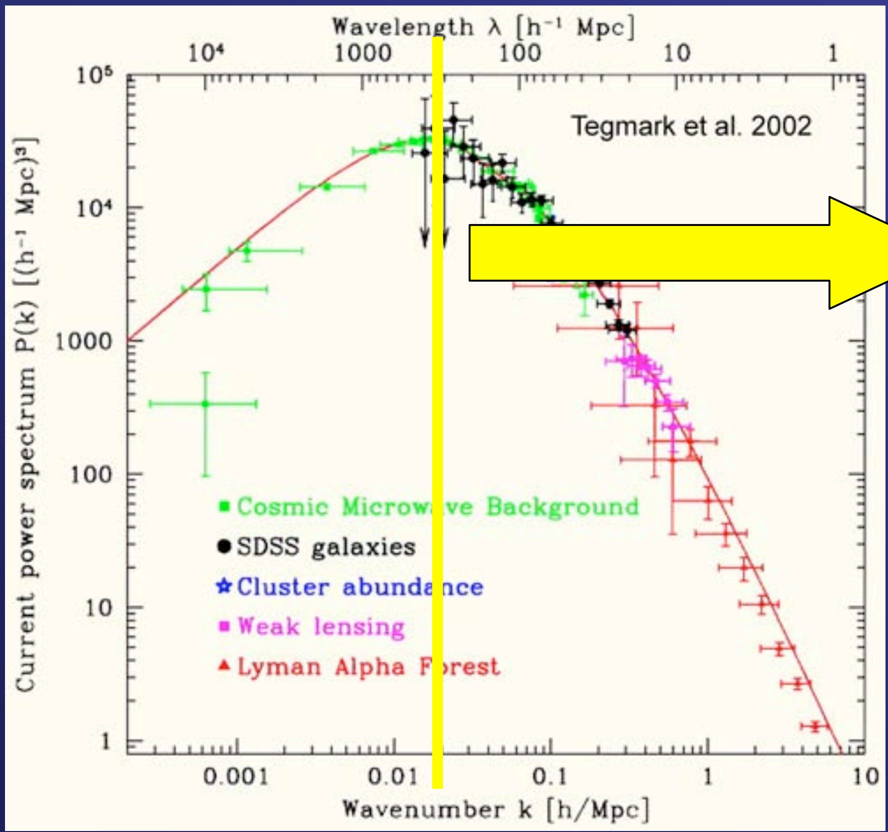

When k_{MAX} becomes larger than the than ~0.01 h/Mpc (peak of power spectrum) there is no gain in further improving the spectral resolution.

Plateau is reached!

BACKGROUND INTENSITY

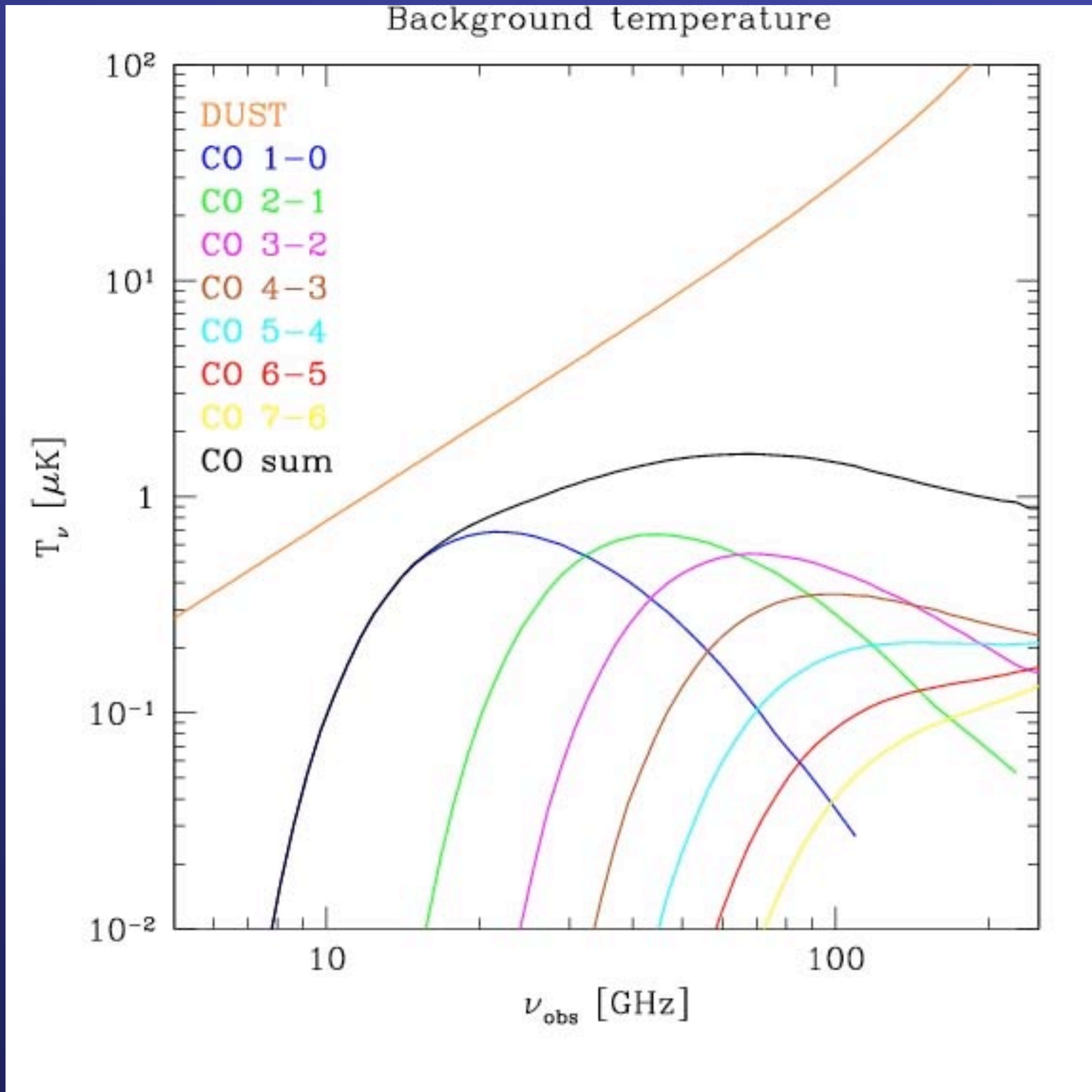

SPECTRAL RESOLUTION

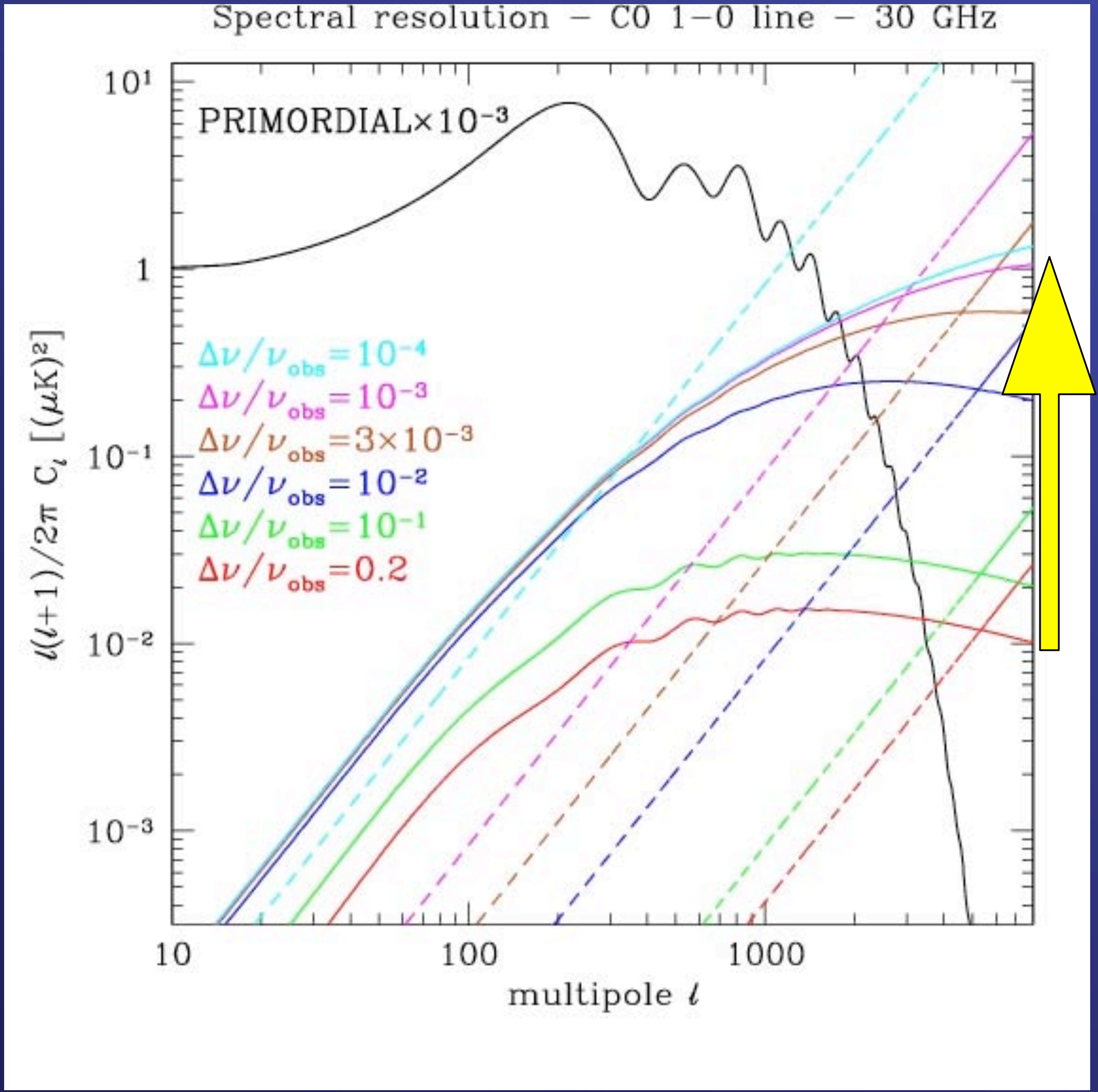

The amplitude of the correlation term grows of ~2 orders of magnitude if the spectral resolution is improved down to $\Delta\nu/\nu_{obs}=10^{-3}$

Primordial fluctuations and other continuum foreground DO NOT DEPEND ON $\Delta\nu/\nu_{obs}$

SOURCE NUMBER COUNTS

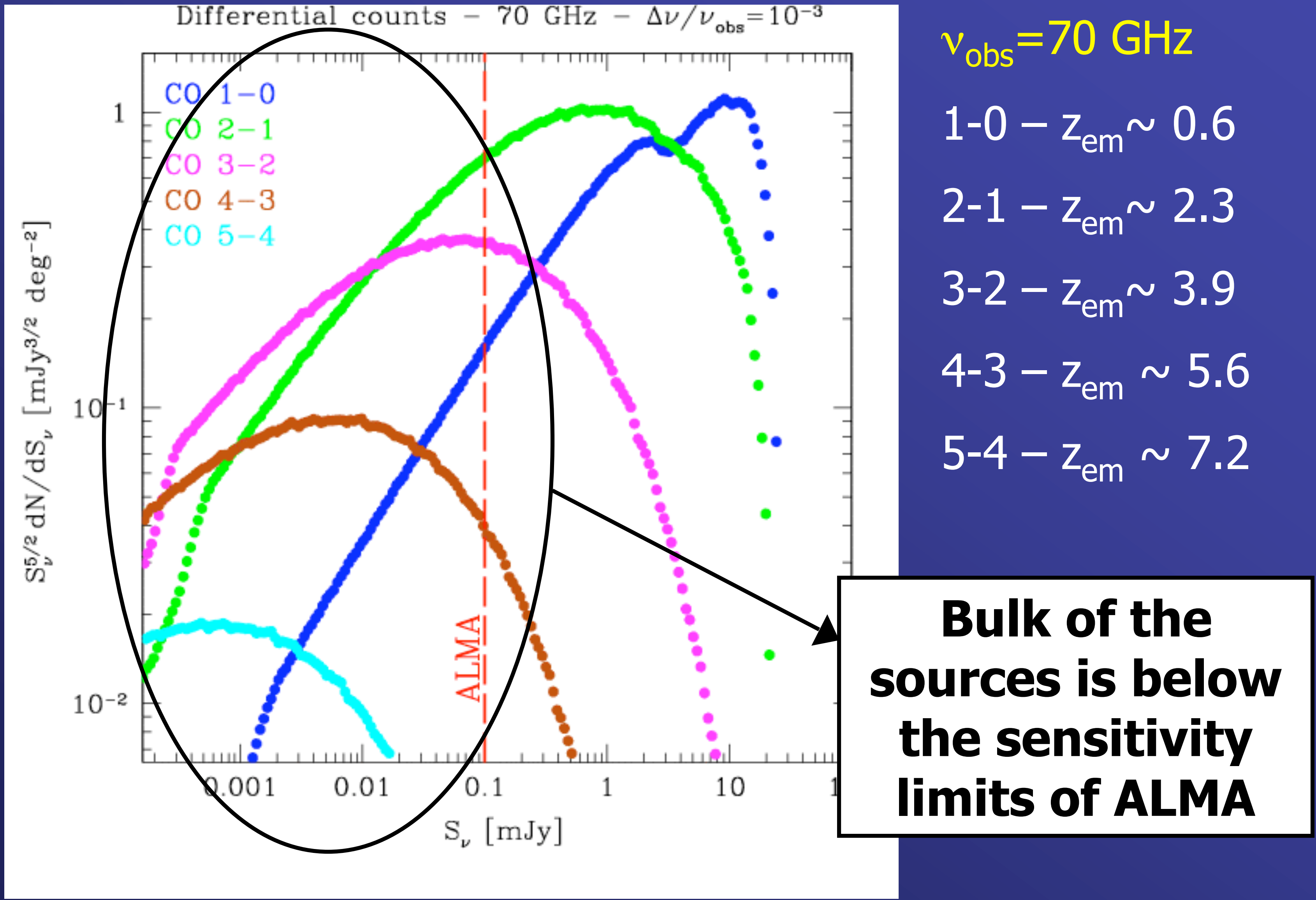

ν_{obs}=70 GHz

1-0 – z_{em}~ 0.6

2-1 – z_{em}~ 2.3

3-2 – z_{em}~ 3.9

4-3 – z_{em} ~ 5.6

5-4 – z_{em} ~ 7.2

SOURCE NUMBER COUNTS

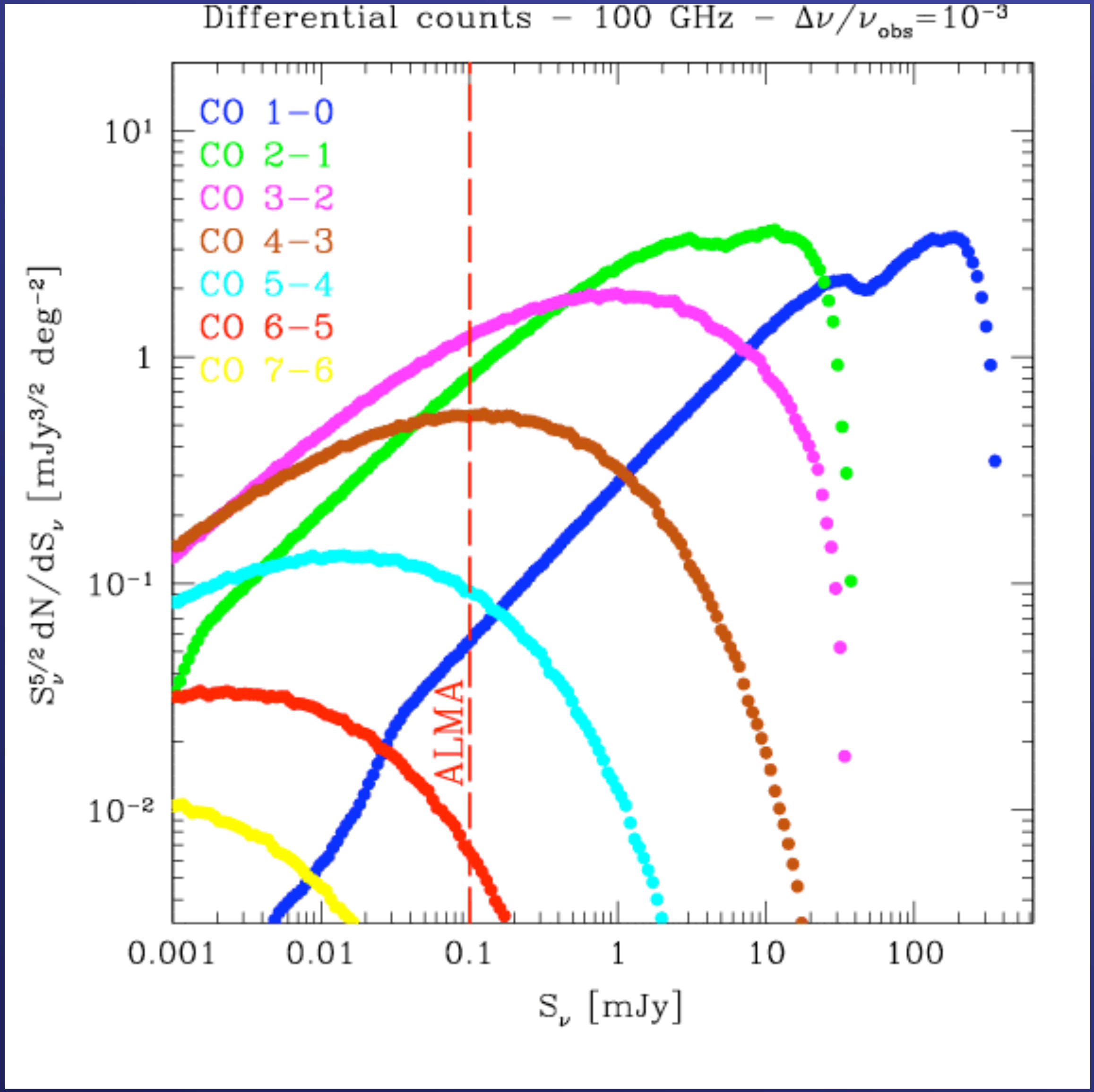

ν_{obs}=100 GHz

1-0 – z_{em}~ 0.2

2-1 – z_{em}~ 1.3

3-2 – z_{em}~ 2.5

4-3 – z_{em} ~ 3.6

5-4 – z_{em} ~ 4.8

6-5 – z_{em} ~ 5.9

7-6 – z_{em} ~ 7.1

RADIO CONTAMINATION

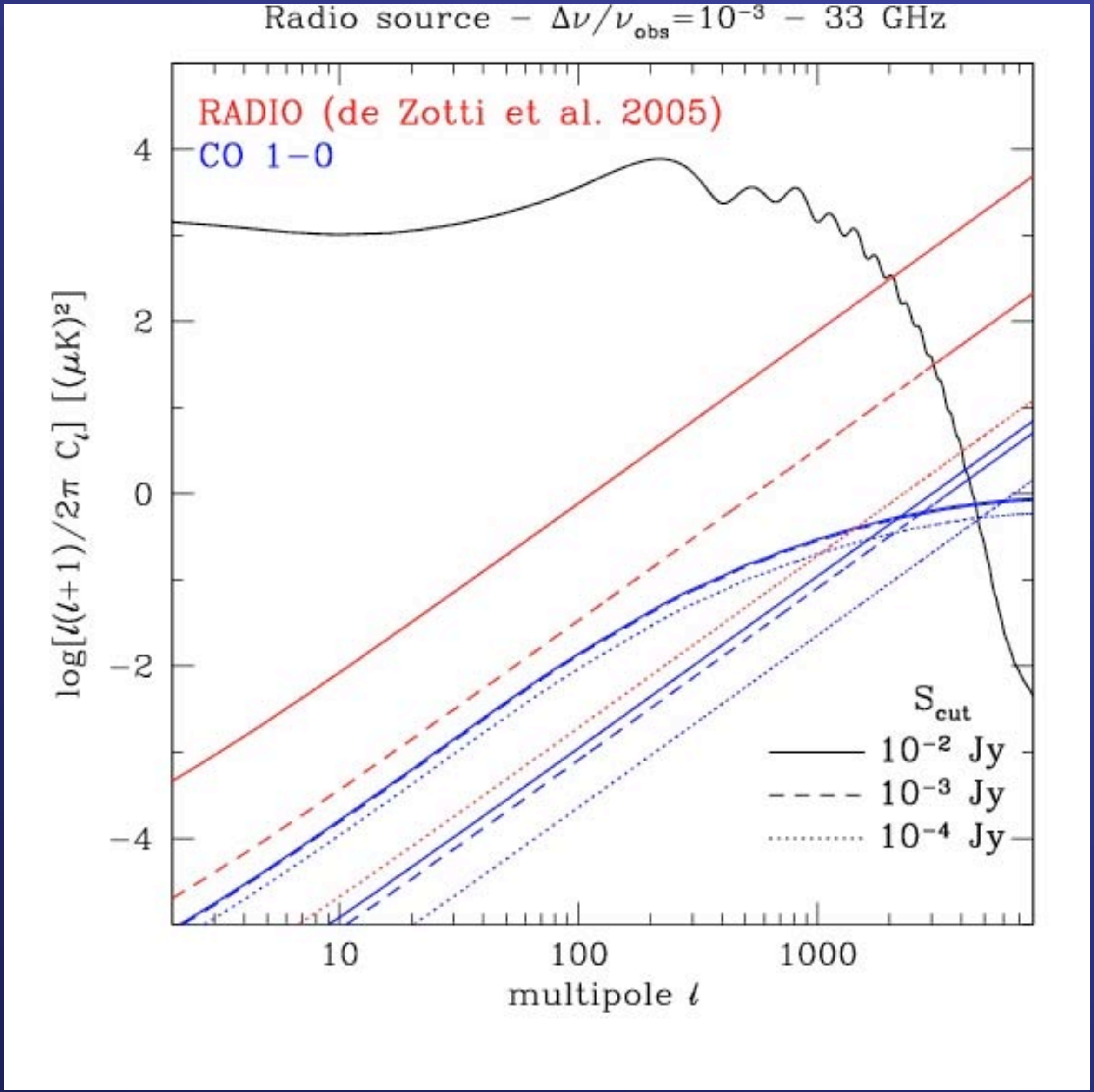

Possibility to decrease the radio contamination by removing bright sources from the maps.

TWO ISSUES

Confusion noise (20-200 sources/deg^2 at 10^{-3}-10^{-4} Jy, should not be a problem)

Clustering properties, not very well known for this population

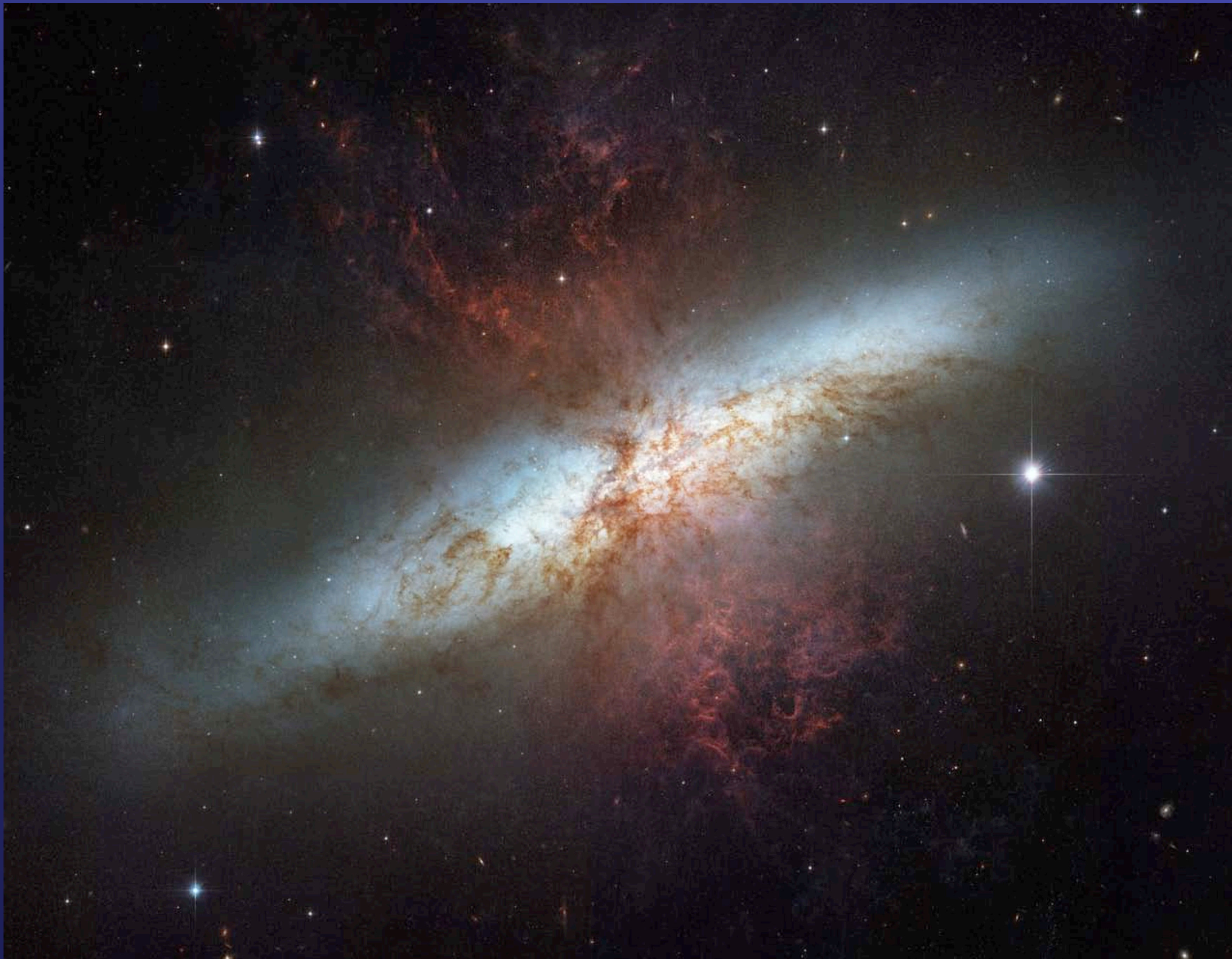

OBSERVATIONAL SAMPLE

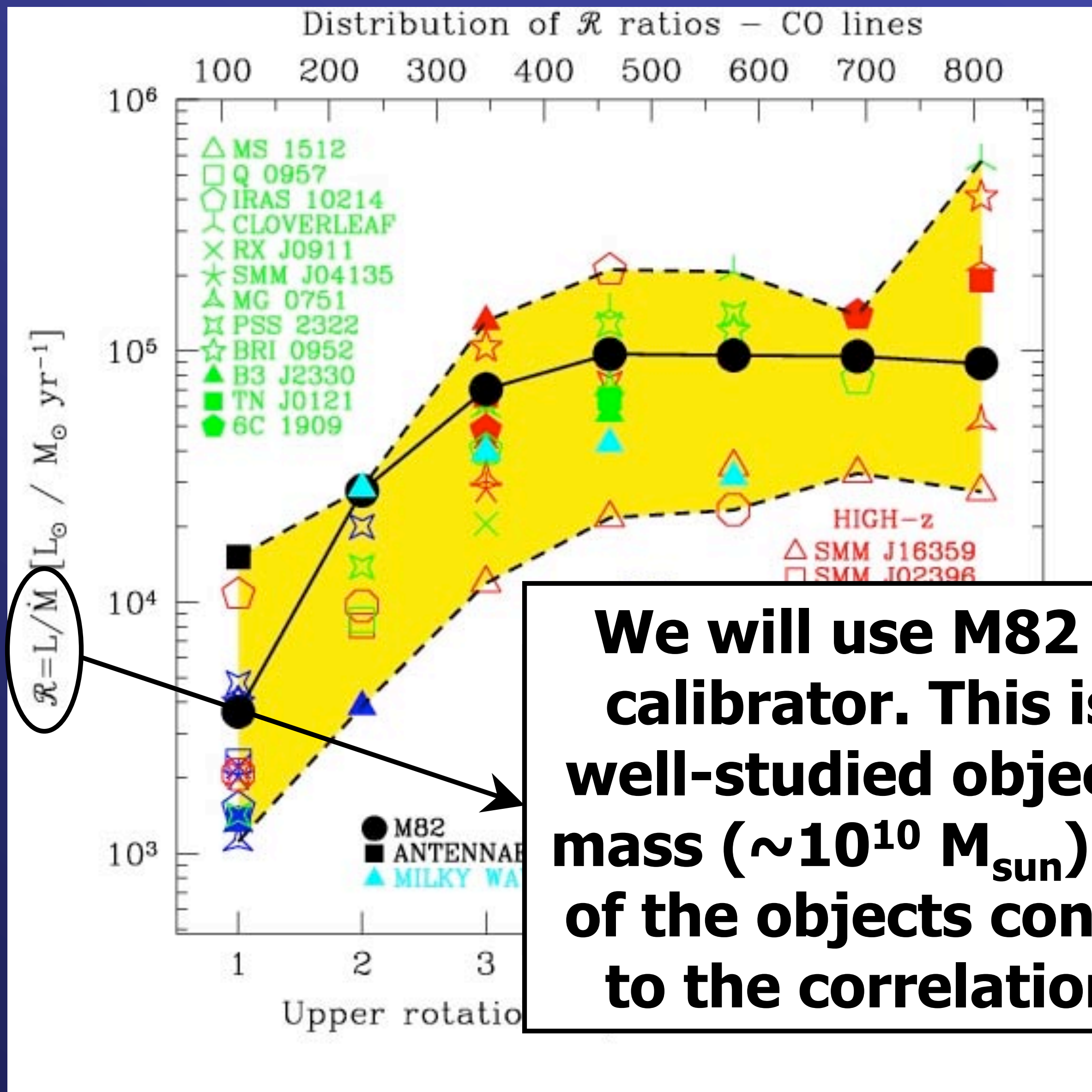

We will use M82 as main calibrator. This is a very well-studied object and its mass (~10^{10} M_{sun}) is typical of the objects contributing to the correlation signal

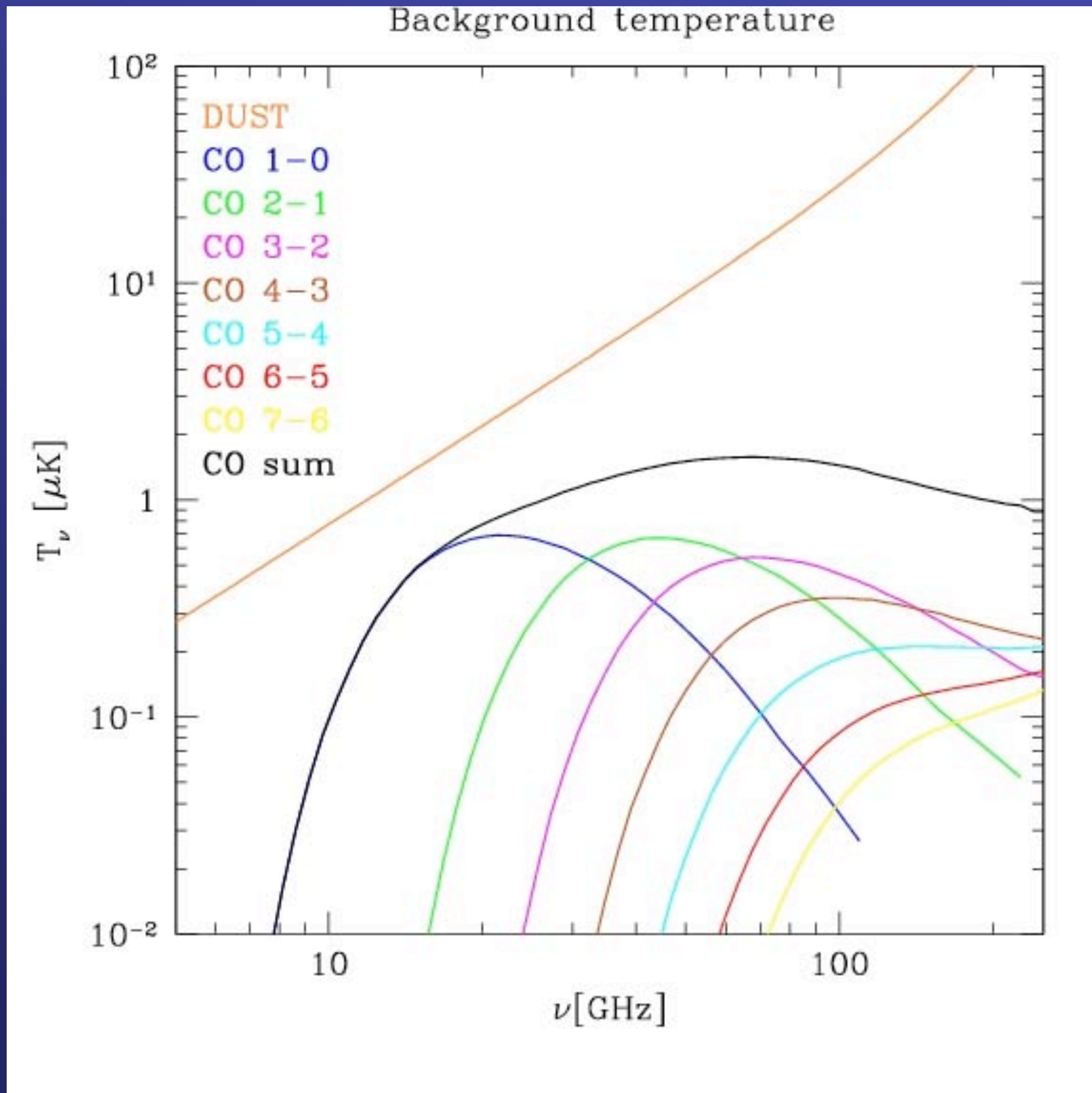

Background temperature
DUST
CO 1−0
CO 2−1
CO 3−2
CO 4−3
CO 5−4
CO 6−5
CO 7−6
CO sum
T_ν [μK]
10^2
10^1
1
10^{-1}
10^{-2}
10
100
ν[GHz]

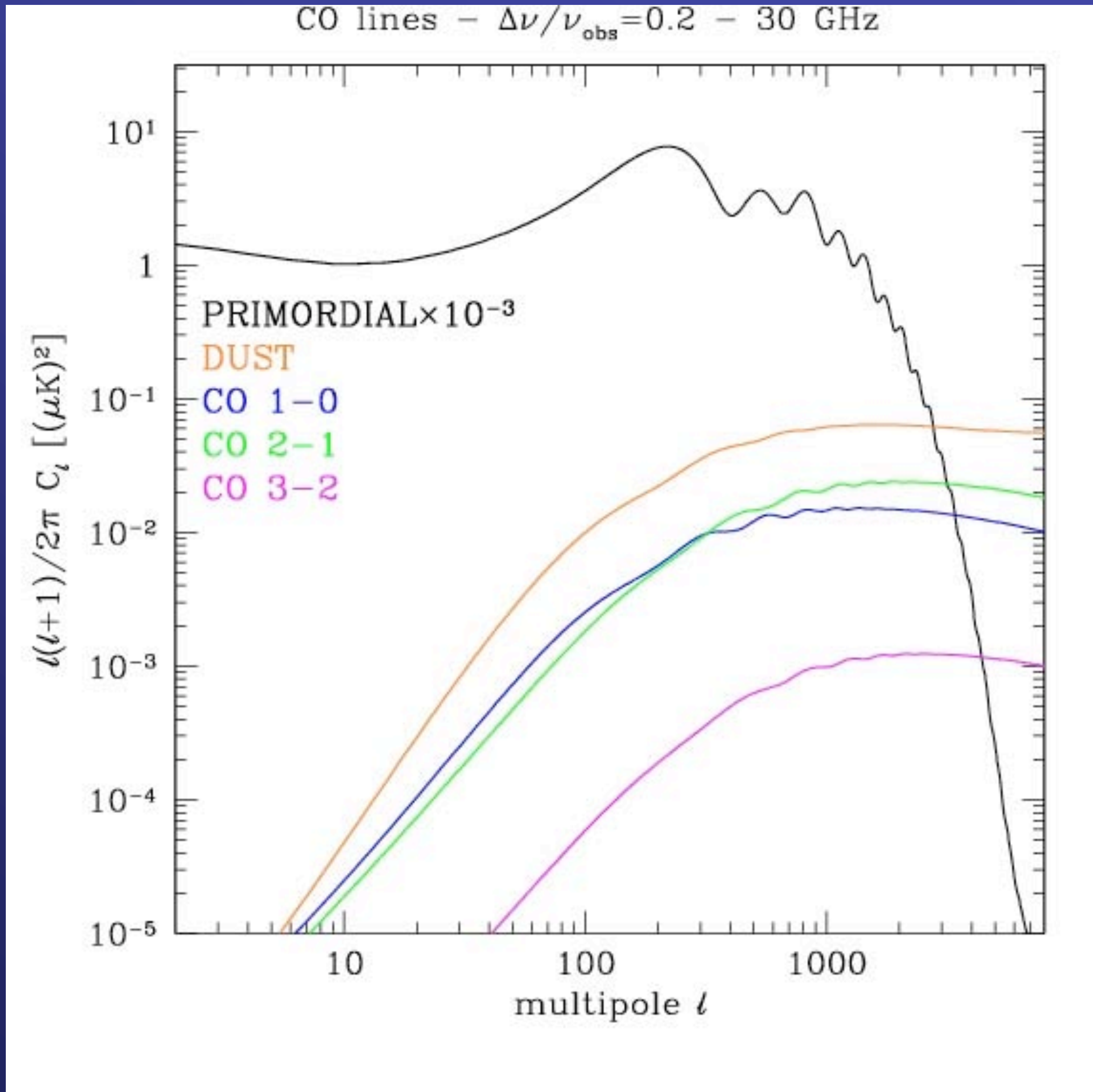
CO lines – Δν/ν_obs=0.2 – 30 GHz
10¹
1
10⁻¹
10⁻²
10⁻³
10⁻⁴
10⁻⁵
ℓ(ℓ+1)/2π C_ℓ [(μK)²]
10
100
1000
multipole ℓ
PRIMORDIAL×10⁻³
DUST
CO 1−0
CO 2−1
CO 3−2

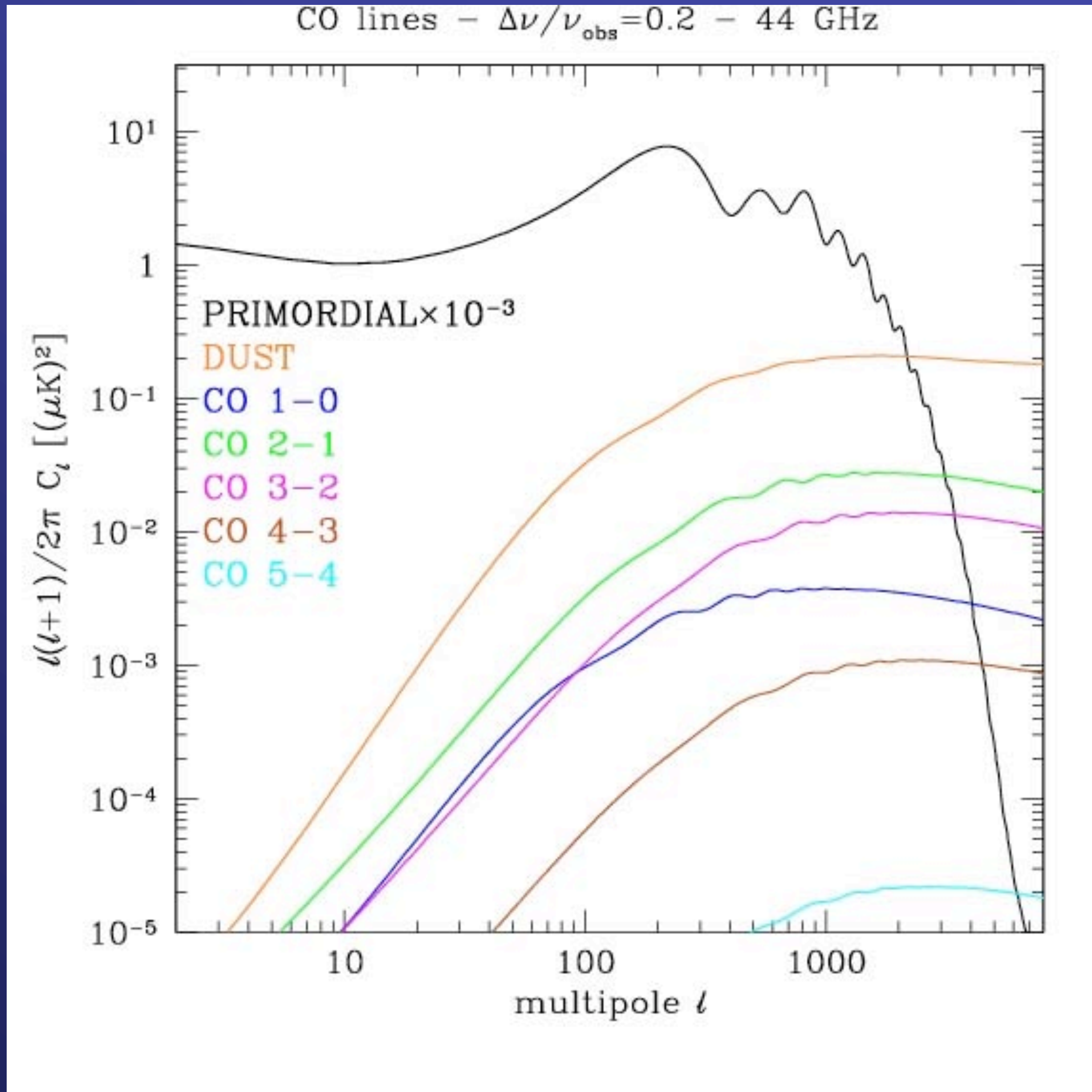

CO lines – Δν/ν_obs=0.2 – 44 GHz
10¹
1
10⁻¹
10⁻²
10⁻³
10⁻⁴
10⁻⁵
ℓ(ℓ+1)/2π C_ℓ [(μK)²]
PRIMORDIAL×10⁻³
DUST
CO 1−0
CO 2−1
CO 3−2
CO 4−3
CO 5−4
10
100
1000
multipole ℓ

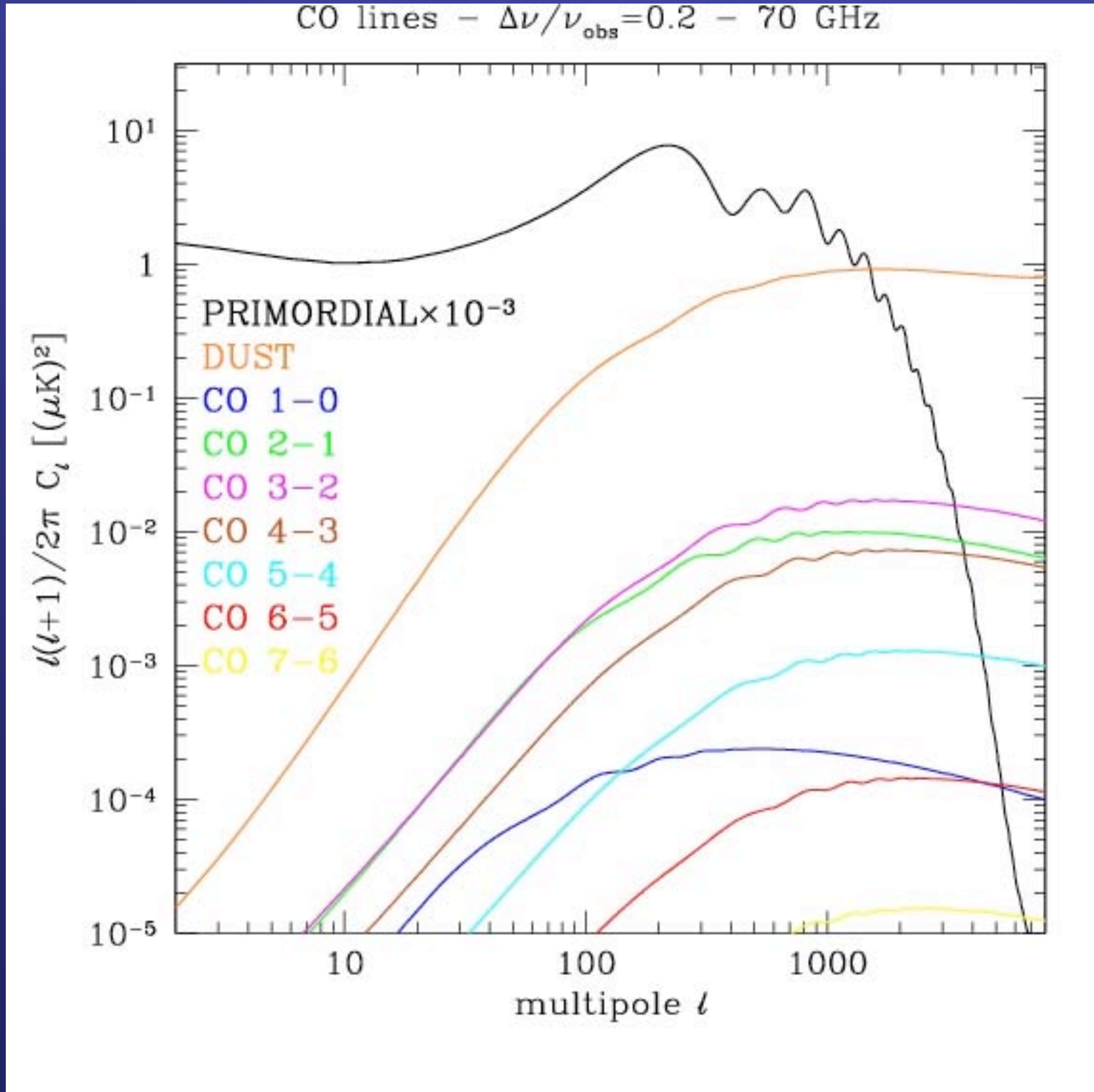
CO lines – $\Delta\nu/\nu_{obs}$=0.2 – 70 GHz
10^1
1
10^{-1}
10^{-2}
10^{-3}
10^{-4}
10^{-5}
PRIMORDIAL×10^{-3}
DUST
CO 1−0
CO 2−1
CO 3−2
CO 4−3
CO 5−4
CO 6−5
CO 7−6
$\ell(\ell+1)/2\pi$ C_ℓ $[(\mu K)^2]$
10
100
1000
multipole ℓ

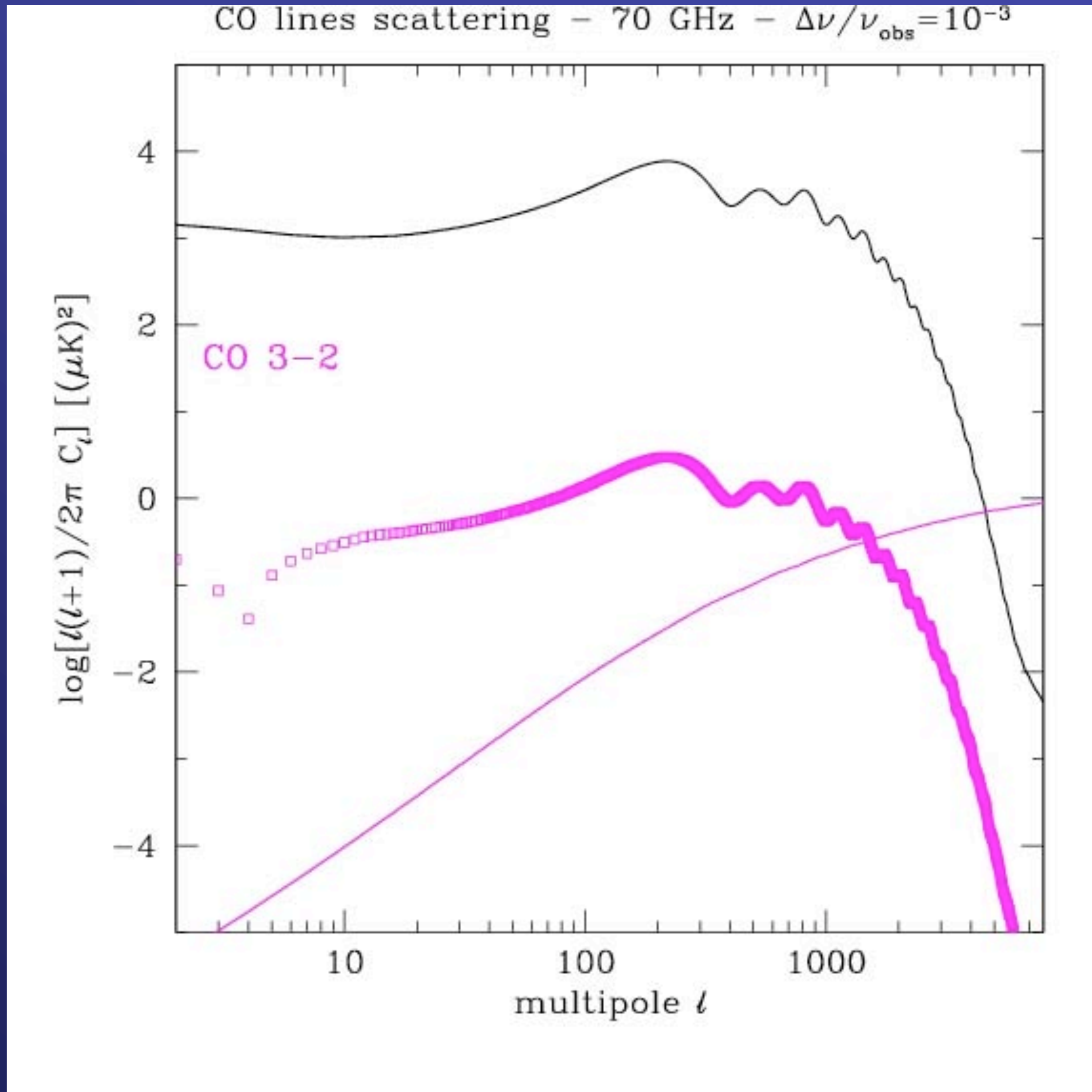

CO lines scattering – 70 GHz – $\Delta\nu/\nu_{obs}=10^{-3}$
CO 3–2
$\log[\ell(\ell+1)/2\pi\ C_\ell]\ [(\mu K)^2]$
4
2
0
−2
−4
10
100
1000
multipole ℓ

Dust spectrum

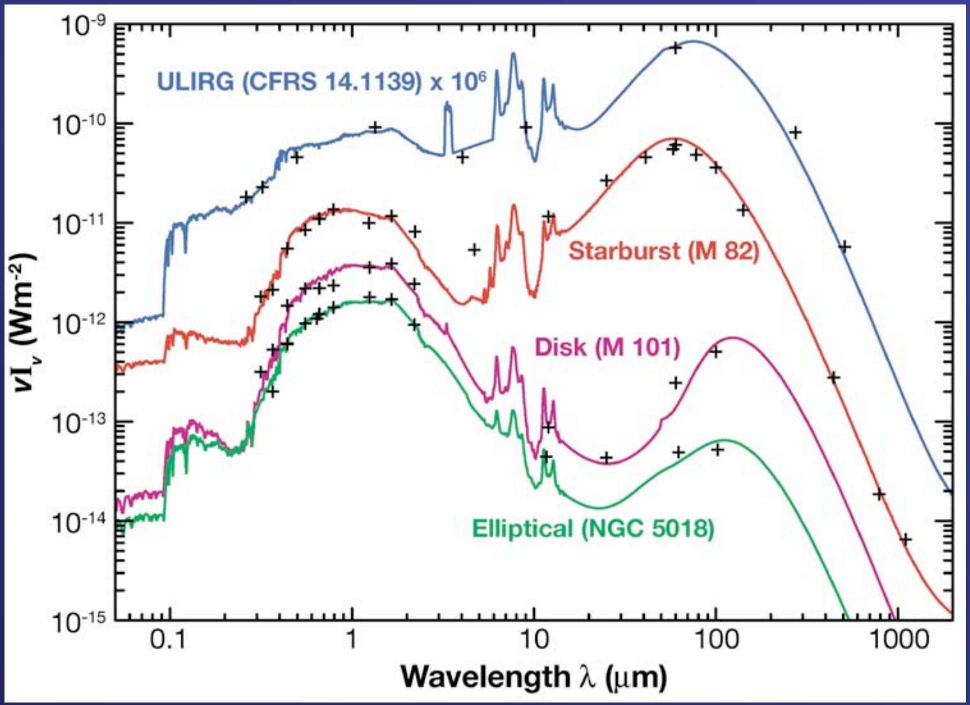

Lagache et al. (2005)

Sub-mm region of the SED of starbursts and ULIRGs is well fitted by a graybody (Blain et al. 02, Chapman et al. 05)

$$L_\nu \propto \nu^\beta B_\nu(T_{dust})$$

Bulk of the emission if due to low-temperature-dust and peaks around 100 μm

Two free parameters: dust temperature T_{dust} and emissivity index β, to be calibrated with the observations (SCUBA)

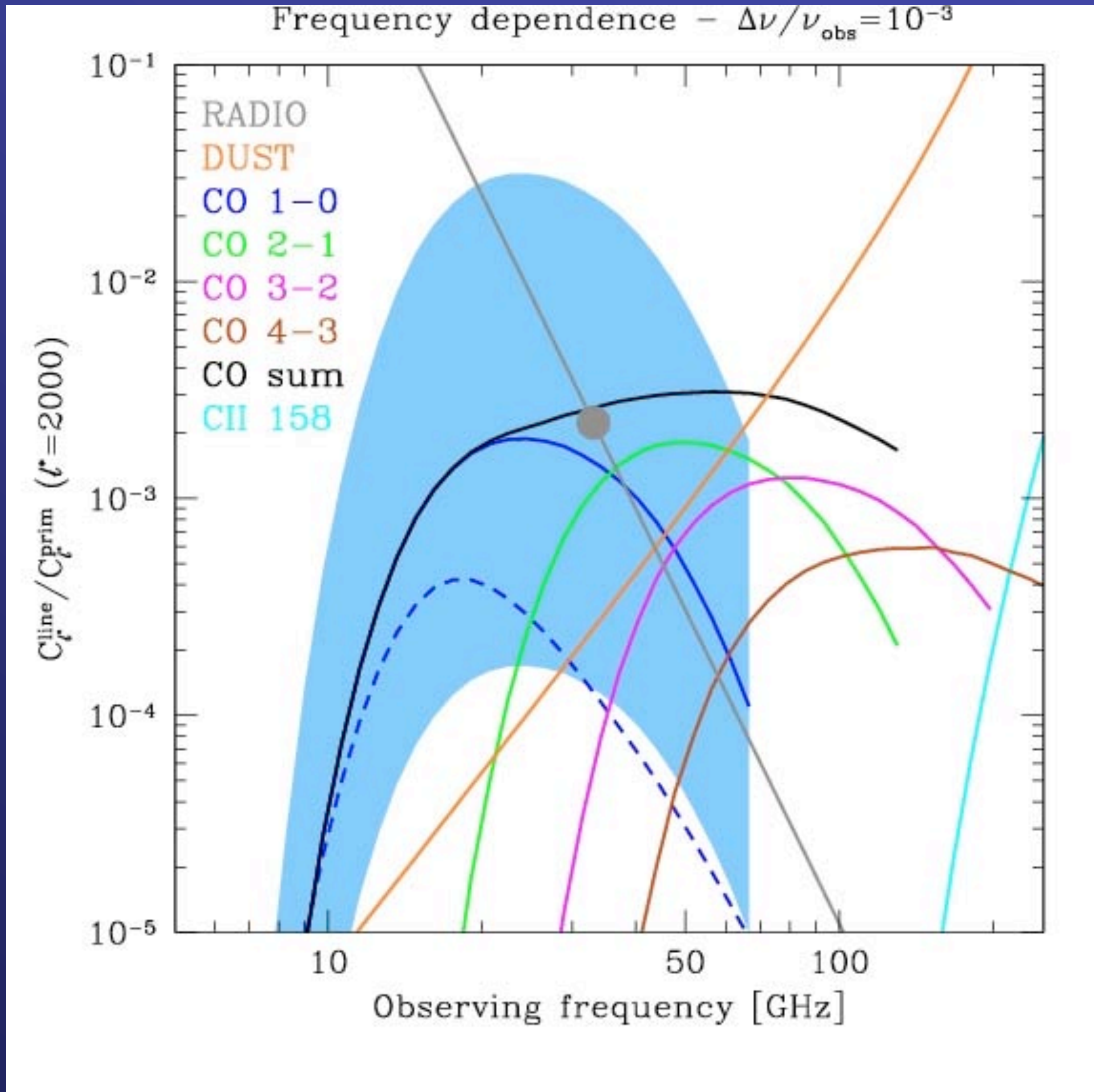

Frequency dependence – $\Delta\nu/\nu_{obs}=10^{-3}$
10^{-1}
10^{-2}
10^{-3}
10^{-4}
10^{-5}
RADIO
DUST
CO 1−0
CO 2−1
CO 3−2
CO 4−3
CO sum
CII 158
$C_\ell^{line}/C_\ell^{prim}$ (ℓ=2000)
10
50
100
Observing frequency [GHz]

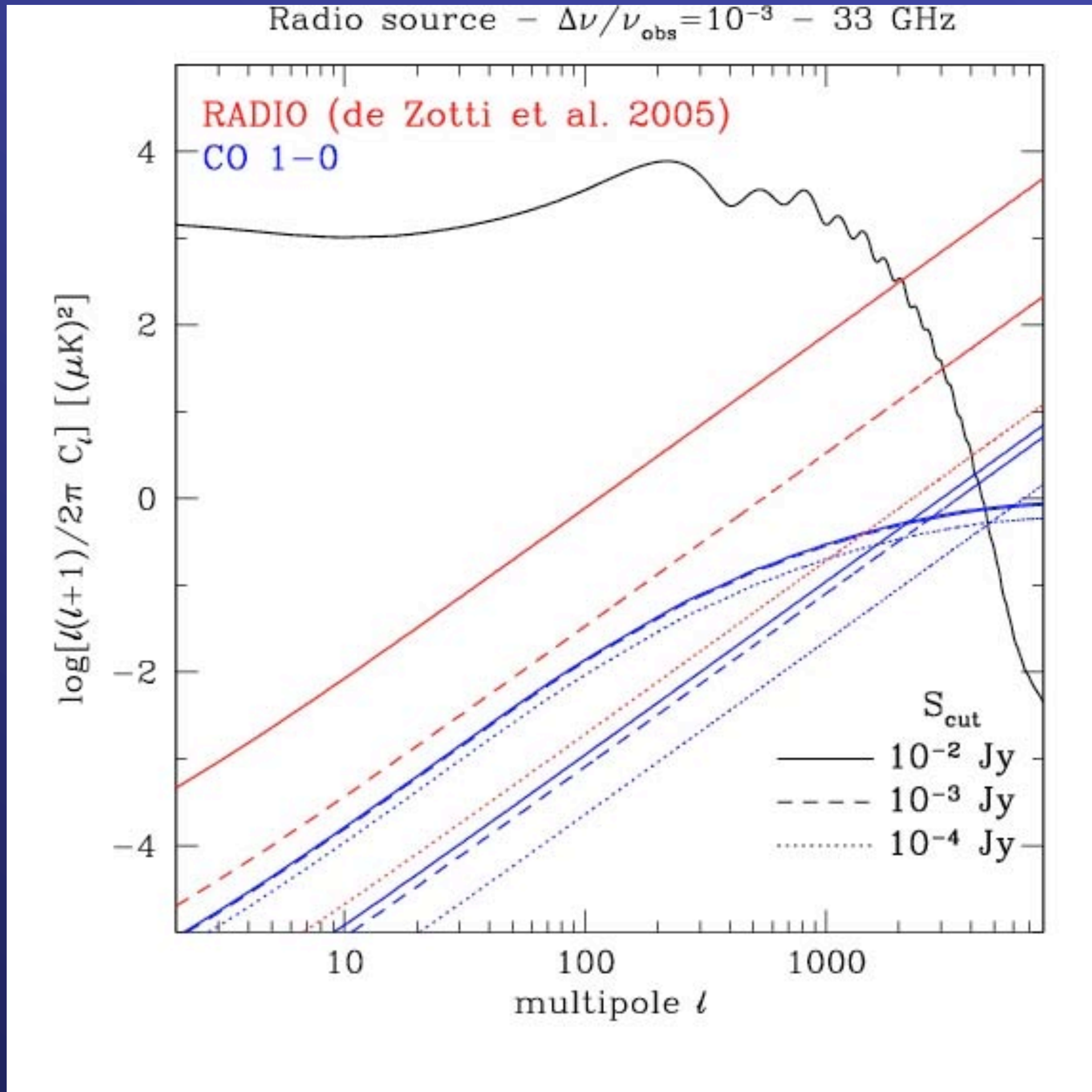
Radio source – $\Delta\nu/\nu_{obs}=10^{-3}$ – 33 GHz
RADIO (de Zotti et al. 2005)
CO 1–0
$\log[\ell(\ell+1)/2\pi\ C_\ell]$ [$(\mu K)^2$]
multipole ℓ
S_{cut}
10^{-2} Jy
10^{-3} Jy
10^{-4} Jy
4
2
0
−2
−4
10
100
1000

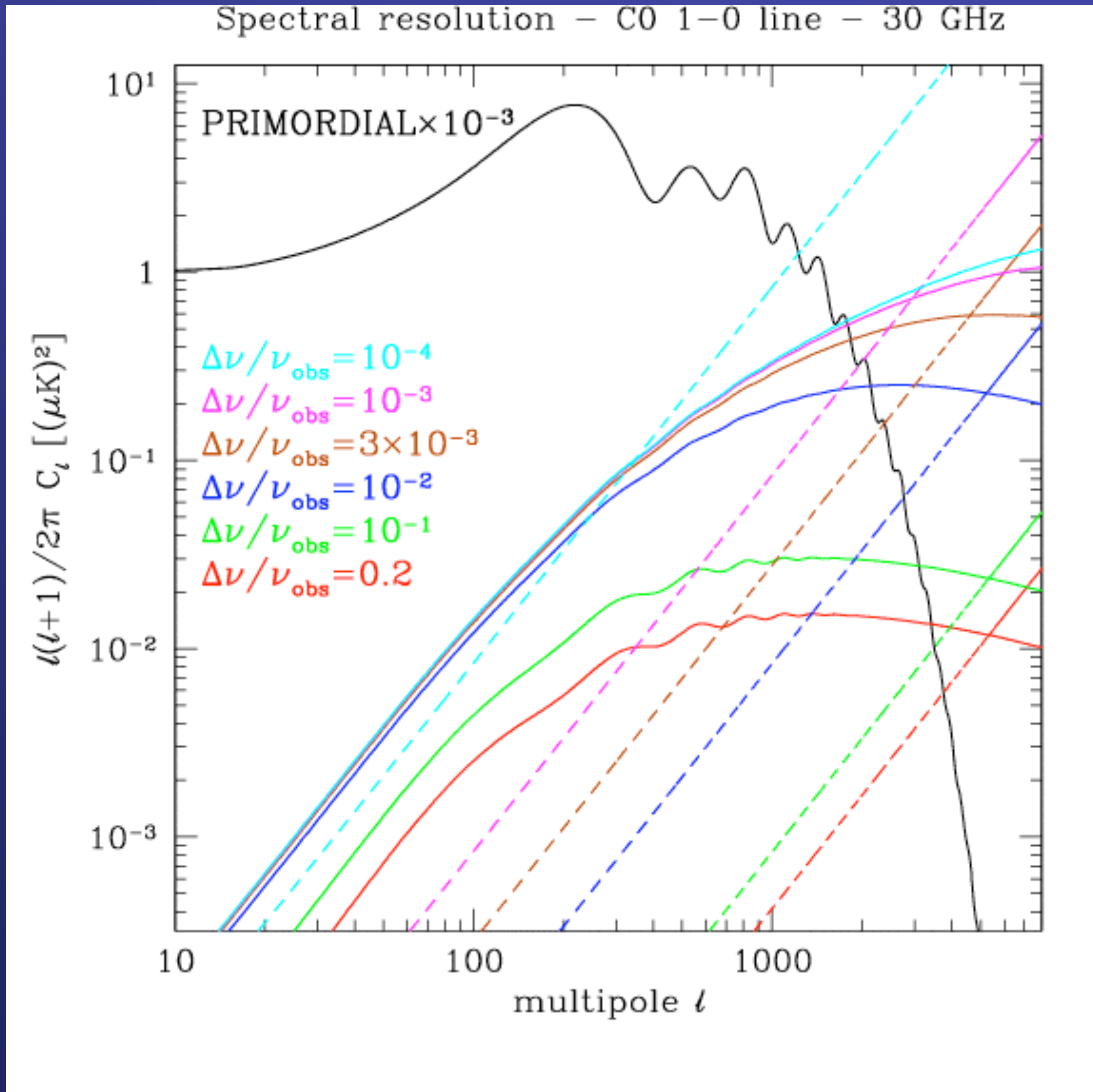
Spectral resolution – CO 1–0 line – 30 GHz
PRIMORDIAL×10⁻³
Δν/ν_obs=10⁻⁴
Δν/ν_obs=10⁻³
Δν/ν_obs=3×10⁻³
Δν/ν_obs=10⁻²
Δν/ν_obs=10⁻¹
Δν/ν_obs=0.2
ℓ(ℓ+1)/2π C_ℓ [(μK)²]
10¹
1
10⁻¹
10⁻²
10⁻³
10
100
1000
multipole ℓ

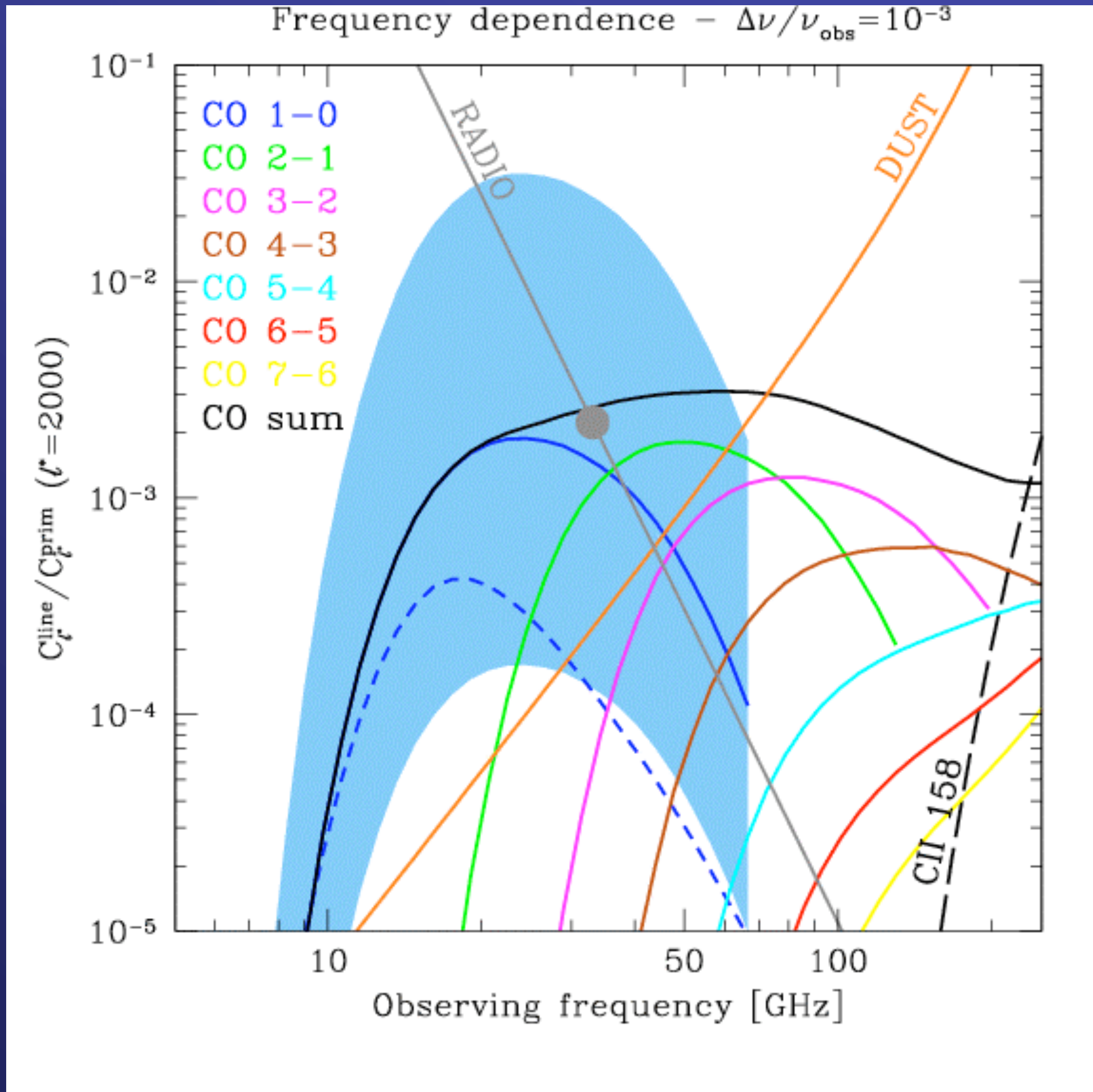

Frequency dependence – $\Delta\nu/\nu_{obs}=10^{-3}$
10^{-1}
10^{-2}
10^{-3}
10^{-4}
10^{-5}
$C_\ell^{line}/C_\ell^{prim}$ (ℓ=2000)
CO 1–0
CO 2–1
CO 3–2
CO 4–3
CO 5–4
CO 6–5
CO 7–6
CO sum
RADIO
DUST
CII 158
10
50
100
Observing frequency [GHz]

Table 1. Luminosities and $\mathcal{R}$ ratios (in boldface) of the CO lines for the local and low-redshift sample of galaxies. The star formation rates are obtained applying the Kennicutt (1998) relation to the far-infrared ($8 - 1000\,\mu$m) luminosity given in the *IRAS revised bright galaxies sample* (Sanders et al. 2003). Distances are from the same catalog: conversion from proper to luminosity distance has been computed using the cosmology-corrected redshift in the Nasa Extragalactic Database (NED). For our Galaxy we use the value of star formation rate given by Cox (2000). The third line in M82 shows the ratio between dust and CO lines luminosities, computed assuming $\Delta\nu/\nu \sim 10^{-3}$ and using the spectrum given by Lagache et al. (2005). References: (a) Weiß et al. (2005b), (b) Gao et al. (2001), (c) Wright et al. (1991), (d) Baan et al. (2008).

Object name	Type	d_L [Mpc]	SFR [$M_\odot$/yr]	CO (1-0) 115.3 GHz [$L_\odot$]	CO (2-1) 230.5 GHz [$L_\odot$]	CO (3-2) 345.8 GHz [$L_\odot$]	CO (4-3) 461.0 GHz [$L_\odot$]	CO (5-4) 576.3 GHz [$L_\odot$]	CO (6-5) 691.5 GHz [$L_\odot$]	CO (7-6) 806.7 GHz [$L_\odot$]
M82	SB	3.63	10.1	3.7×10^4 a	2.8×10^5 a	7.1×10^5 a	9.8×10^5 a	9.7×10^5 a	9.6×10^5 a	9.0×10^5 a
				$\mathbf{3.7\times10^3}$	$\mathbf{2.8\times10^4}$	$\mathbf{7.0\times10^4}$	$\mathbf{9.7\times10^4}$	$\mathbf{9.6\times10^4}$	$\mathbf{9.5\times10^4}$	$\mathbf{8.9\times10^4}$
		M82 L_{dust}/L_{CO} ratio:			0.005	0.009	0.02	0.05	0.12	0.24
Antennae	SB	21.8	11.8	1.8×10^5 b						
				$\mathbf{1.5\times10^4}$						
Milky Way		-	3.0		8.5×10^4 c	1.2×10^5 c	1.3×10^5 c	9.5×10^4 c		
					$\mathbf{2.8\times10^4}$	$\mathbf{4.0\times10^4}$	$\mathbf{4.3\times10^4}$	$\mathbf{3.2\times10^4}$		
IRAS 01077-1707		145	72.9	2.9×10^5 d						
				$\mathbf{4.0\times10^3}$						
IRAS 01364-1042		207	98.4	2.3×10^5 d						
				$\mathbf{2.3\times10^3}$						
IRAS 04454-4838		220	105	1.6×10^5 d						
				$\mathbf{1.5\times10^3}$						
IRAS 08520-6850		205	98.4	1.3×10^5 d						
				$\mathbf{1.3\times10^3}$						
IRAS 09111-1007		243	171	3.8×10^5 d						
				$\mathbf{2.2\times10^3}$						
IRAS 14348-1447	SB	388	341	6.9×10^5 d						
				$\mathbf{2.0\times10^3}$						
IRAS 14378-3651		315	242	2.7×10^5 d						
				$\mathbf{1.1\times10^3}$						
IRAS 18293-3413		80.6	110	5.3×10^5 d	2.2×10^6 d					
				$\mathbf{4.8\times10^3}$	$\mathbf{2.0\times10^4}$					
IRAS 19115-2124		216	127	5.1×10^5 d						
				$\mathbf{4.0\times10^3}$						
IRAS 20550+1656		136	127	1.7×10^5 d	4.8×10^5 d					
				$\mathbf{1.3\times10^3}$	$\mathbf{3.8\times10^3}$					
IRAS 22491-1808	SB	350	220	3.0×10^5 d						
				$\mathbf{1.4\times10^3}$						

Table 2. Luminosities and $\mathcal{R}$ ratios (in boldface) of the CO lines for the high-redshift sample of galaxies. Luminosities of the lensed sources (marked with $\star$) are corrected with the magnification factors given in Greve et al. (2005) and Solomon & Vanden Bout (2005). Where more than one observation were available we assumed an average between them. References: (a) Kneib et al. (2004), (b) Weiß et al. (2005a), (c) Sheth et al. (2004), (d) Kneib et al. (2005), (e) Solomon & Vanden Bout (2005), (f) Greve et al. (2005), (g) Hainline et al. (2006), (h) Tacconi et al. (2006), (i) Kovács et al. (2006), (j) Neri et al. (2003), (k) Genzel et al. (2003), (l) Frayer et al. (1999), (m) Downes & Solomon (2003), (n) Takata et al. (2006), (o) Greve et al. (2003), (p) Andreani et al. (2000), (q) Frayer et al. (2008), (r) Baker et al. (2004), (s) Planesas et al. (1999), (t) Brown & Vanden Bout (1991), (u) Solomon et al. (1992b), (v) Solomon et al. (1992a), (w) Downes et al. (1995), (x) Barvainis et al. (1994), (y) Wilner et al. (1995), (z) Barvainis et al. (1997), (aa) Weiß et al. (2003), (ab) Hainline et al. (2004), (ac) Barvainis et al. (2002), (ad) Carilli et al. (2002), (ae) Cox et al. (2002), (af) Guilloteau et al. (1999), (ag) De Breuck et al. (2003a), (ah) De Breuck et al. (2003b), (ai) Papadopoulos et al. (2000).

Object name	Type	z	SFR $[M_\odot/yr]$	CO (1-0) 115.3 GHz $[L_\odot]$	CO (2-1) 230.5 GHz $[L_\odot]$	CO (3-2) 345.8 GHz $[L_\odot]$	CO (4-3) 461.0 GHz $[L_\odot]$	CO (5-4) 576.3 GHz $[L_\odot]$	CO (6-5) 691.5 GHz $[L_\odot]$	CO (7-6) 806.7 GHz $[L_\odot]$
SMM J16359$\star$	SB	2.52	500 a			6.0×10^6 b-d **1.2×10^4**	1.1×10^7 b **2.2×10^4**	1.7×10^7 b **3.4×10^4**	1.6×10^7 b **3.2×10^4**	1.4×10^7 b **2.8×10^4**
SMM J02396$\star$	AGN	1.06	975 e		7.9×10^6 f **8.1×10^3**					
SMM J13120	AGN	3.41	810 g	1.0×10^7 g **1.2×10^4**			1.7×10^8 f **2.1×10^5**			
SMM J16366	SB	2.45	1455 i			7.7×10^7 f,h **5.3×10^4**				3.3×10^8 h **2.3×10^5**
SMM J16371	SB+AGN	2.38	877 i			4.0×10^7 f **4.6×10^4**				
SMM J22174	SB	3.10	1800 e			5.1×10^7 f **2.8×10^4**				
SMM J04431$\star$	SB+AGN	2.51	450 e			1.4×10^7 h,j **3.1×10^4**				2.4×10^7 h **5.3×10^4**
SMM J09431$\star$	SB+AGN	3.35	1200 g	$< 2.5\times10^6$ g **$< 2.1\times10^3$**			8.9×10^7 h,j **7.4×10^4**			
SMM J16368	SB+AGN	2.38	897 i			9.3×10^7 h,j **1.0×10^5**				3.7×10^8 h,j **4.1×10^5**
SMM J02399$\star$	SB+AGN	2.80	500 k			6.6×10^7 k,l **1.3×10^5**				
SMM J14011$\star$	SB	2.56	360 e			2.4×10^7 l,m **6.7×10^4**				6.9×10^7 m **1.9×10^5**
SMM J123549	SB+AGN	2.20	1163 n			5.6×10^7 h **4.8×10^4**			1.6×10^8 h **1.4×10^5**	
ERO J16450	SB	1.44	1539 o	3.2×10^6 o **2.1×10^3**	1.5×10^7 d **9.7×10^3**			3.6×10^7 p **2.3×10^4**		
GOODS J123634	SB	1.22	950 q		2.6×10^7 q **2.8×10^4**					
MS 1512$\star$	LBG	2.73	15 e			5.9×10^5 r **4.0×10^4**				
Q 0957$\star$	QSO	1.41	900 e		7.6×10^6 s **8.5×10^3**					
IRAS F10214$\star$	QSO	2.29	540 e			2.2×10^7 t-w **4.0×10^4**			4.2×10^7 v **$7,7\times10^4$**	
CLOVERLEAF$\star$	QSO	2.56	810 e			4.8×10^7 x-aa **5.9×10^4**	1.2×10^8 z **1.5×10^5**	1.7×10^8 z **2.1×10^5**		4.6×10^8 z **5.7×10^5**
RX J0911$\star$	QSO	2.80	345 e			7.1×10^6 ab **2.1×10^4**				
SMM J04135$\star$	QSO	2.84	3600 e			2.3×10^8 ab **6.4×10^4**				
MG 0751$\star$	QSO	3.20	435 e				3.2×10^7 ac **7.2×10^4**			
PSS J2322$\star$	QSO	4.11	1800 e	2.6×10^6 ad **1.4×10^3**	2.5×10^7 ad **1.4×10^4**	2.3×10^8 ae **1.3×10^5**		2.5×10^8 ae **1.4×10^5**		
BRI 0952$\star$	QSO	4.43	360 e					4.3×10^7 af **1.5×10^5**		
B3 J2330	HzRG	3.09	1950 e				1.1×10^8 ag **5.6×10^4**			
TN J0121	HzRG	3.52	1050 e				1.3×10^8 ah **1.2×10^5**			
6C 1909	HzRG	3.54	1470 e				1.7×10^8 ai **1.2×10^5**			

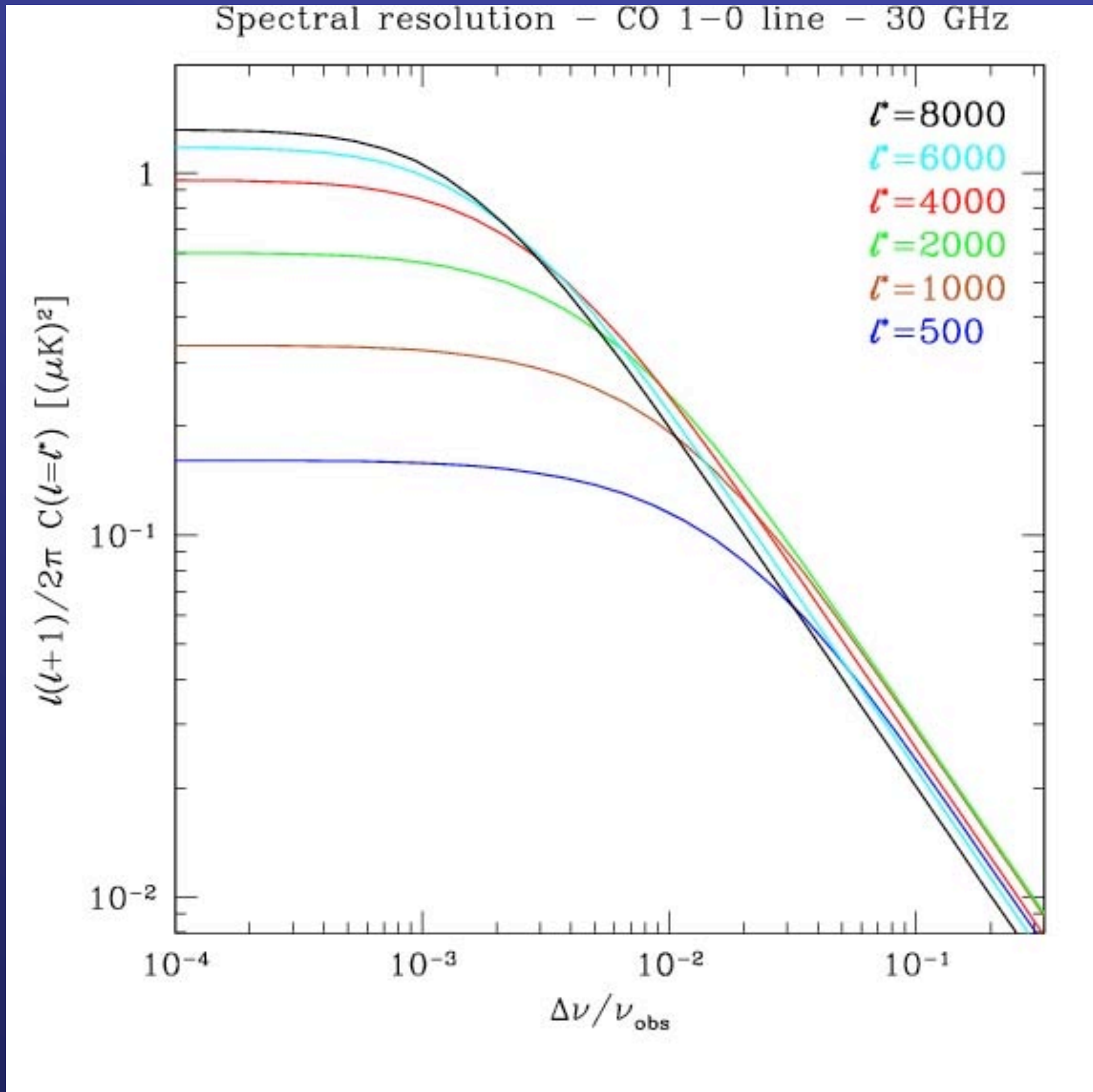

Several measurements with different spectral resolution will permit to separate narrow line contribution from foregrounds with continuum spectrum